Aerodynamics of wind turbine wakes

Literature review

B. Sanderse

CWI

Abstract

This report reviews the available literature on the aerodynamics of wind turbines and wind farms. Firstly, two introductory chapters are devoted to the physics of the flow around a wind turbine and the existing engineering models for blade and wake aerodynamics. The focus of this work is however on the numerical modeling of wakes. The difficulties in solving the Navier-Stokes equations are discussed, and the different existing models for the description of the rotor and the wake are mentioned, along with problems associated with the choice of turbulence models and inflow conditions.

The purpose of this overview is to include the latest developments in the numerical computation of wind turbine aerodynamics.

Contents

1 Introduction

1.1 Simulating wind turbine wakes in wind farms

During the last decades more and more wind turbines have been installed in large wind farms. The grouping of turbines in such a farm introduces two major issues: a wind turbine operating in the wake of another turbine has a reduced power production (because of a lower incident wind speed) and shortens the lifetime of the rotors (because of an increased turbulence intensity) [11]. For example, Neustadter and Spera [53] found a reduction of 10% in power output for three turbines separated by 7 rotor diameters; Elliott mentions in his review [22] a 'considerable reduction in efficiency' and '[the windfarm] produced substantially less energy'. For full wake conditions power losses of downstream turbines can be 30-40%, but when averaged over different wind directions, losses of 5-8% have been reported [4, 5].

In order to reduces power losses and to improve the lifetime of the blades it is necessary to obtain a good understanding of the behavior of wind turbine wakes in wind farms. Such an understanding can be obtained by numerical or experimental *simulation*. Three tasks can be defined for simulating wind turbine wakes:

1 Calculating rotor performance and park efficiency; this requires the time-averaged velocity profile behind a turbine.

2 Calculating blade loading of turbines operating in wakes of other turbines and the fluctuations in the electrical energy output; this requires the turbulence fluctuations and the turbulence intensity in the wake.

3 Calculating wake meandering; this requires that large atmospheric eddies are taken into account.

There are a number of reasons for focusing on numerical simulation instead of on experiments:

- Full-scale, good quality experiments are costly and have been limited mainly to provide global information on the flow field. Computational Fluid Dynamics (CFD) can provide detailed information both upstream and downstream of the turbine.

- Due to the variability in atmospheric conditions it is difficult to find the mutual influence of turbines on each other.

- Optimization of a wind farm layout in an experimental setting is almost impossible.

However, CFD computations of wind farms face other difficulties:

- Accurately modeling both the flow over the turbine blades and the flow in the near and far wake requires massive computer resources, due to the *unsteady*, *turbulent* character of the flow. For most turbines the optimal operating condition is close to stall. The flow field exhibits scales that range from the size of small eddies in the boundary layer on the blade to the distance between wind turbines. Simulating the turbulence in the flow accurately and preventing artificial diffusion is an ongoing challenge.

- The rotation of the rotor blades leads to severe problems in constructing a computational grid.

Since the review of Vermeer et al. [81] many studies have appeared that address these issues. CFD is now used by many researchers in the wind industry, and in order to obtain an overview of the most important work this report gives an overview of the latest developments in the numerical computation of wind turbines.

1.2 Outline of this report

Before discussing the different existing numerical models for simulating the flow around wind turbines, it is important to understand the physics of the flow. Therefore, chapter 2 gives an overview of the aerodynamics of a wind turbine, including a description of the atmospheric effects that influence its working. Simplified models are used to explain the basic aerodynamic concepts. In chapter 3 we will look at more complicated models, what we call 'engineering models', that exist for designing wind turbines and wind farms. Readers with a background in wind turbine or wind farm aerodynamics might skip these two chapters. Chapter 4 considers even more advanced models for simulating flows around wind turbines which are based on CFD. Chapter 5 discusses the possibilities and problems associated with optimizing wind farms. Chapter 6 contains a summary of this literature survey.

A number of sources are used throughout this report, and will not be mentioned continuously:

- The reviews of Snel [65, 66], the extensive review on wake aerodynamics by Vermeer et al. [81], the review on wake modeling by Crespo et al. [16] and the review of van der Pijl [78].

- The books of Burton et al. [10] and Hansen [24].

2 Aerodynamics of wind turbines

The purpose of this chapter is to give an overview of the most important aspects of the aerodynamics of wind turbines. A good understanding of the physics of the flow helps to understand the choice for a mathematical model.

2.1 Characteristics of the atmosphere

Wind turbines are operating in the lowest part of the atmospheric boundary layer of the Earth. This severely complicates the calculation of the flow around them. Some properties and nomenclature of the atmosphere are therefore presented in this section.

2.1.1 Atmospheric boundary layer

The velocity profile of the atmospheric boundary layer (ABL) is often modeled by a logarithmic approximation:

$$\bar{u}(z) \propto \ln(z/z_0), \tag{1}$$

with z_0 the surface roughness length, ranging from 0.001m (rough sea) to 0.03m for open farmland with few trees to tens of meters for urban areas. If besides roughness the Coriolis effect is also taken into account the boundary layer is given by:

$$\bar{u}(z) = u^*(\ln(z/z_0) + \Psi)/\kappa, \tag{2}$$

with u^* the friction velocity (defined by $u^* = \sqrt{\tau_w/\rho}$, with τ_w the wall shear stress), κ the von Kármán constant (~ 0.4) and Ψ a function depending on stability (stability is discussed in section 2.1.2). For a neutral atmosphere one might take $\Psi = 34.5 f z/u^*$, with $f = 2\Omega \sin|\lambda|$ the Coriolis parameter, depending on the Earth's rotational speed Ω and latitude λ.

Alternatively, a power law approximation is often used:

$$\bar{u}(z) \propto z^\alpha, \tag{3}$$

where $\bar{u}$ is the mean wind speed and $\alpha \approx 0.14$ [10], or 0.1-0.25 [24]. With a given mean wind speed $\bar{u}(H)$ at hub height H the boundary layer profile is determined as

$$\bar{u}(z) = \bar{u}(H) \left(\frac{z}{H}\right)^\alpha. \tag{4}$$

Although this is a convenient expression, it has no theoretical basis (in contrast to the logarithmic profile).

The height of the (velocity) boundary layer can range from approximately hundred meters to a few kilometers. The definition of this height is sometimes taken as the distance above the Earth where turbulence disappears; it is hard to define the height as a percentage of the undisturbed flow (as is done in aerospace applications), because the undisturbed flow is not defined. Above the boundary layer the geostrophic wind is encountered, driven by pressure gradients and influenced by the Coriolis force.

2.1.2 Stability

The height of the atmospheric boundary layer and the turbulence intensity depend on the thermal stratification, see e.g. [6, 10, 46, 56]. For analyzing atmospheric stability the concept of the

adiabatic lapse rate is useful. The adiabatic lapse rate is the change in temperature with height for a system with no heat exchange, $\left(\frac{dT}{dz}\right)_{ad}$, and is approximately $-1°C$ per 100m. The stability of the atmosphere depends on the actual lapse rate $\frac{dT}{dz}$, which has an average of $-0.65°C$ per 100m. The following atmospheric boundary layers may be considered:

- *unstable*: normally during daytime, surface heating causes air to rise, forming large convection cells ($\frac{dT}{dz} < \left(\frac{dT}{dz}\right)_{ad}$). When the surrounding air is still colder (no thermal equilibrium), this results in large-scale turbulent eddies and a thick boundary layer; the stratification is unstable.

- *stable*: when surface cooling suppresses vertical motion of the air, turbulence effects are not caused by large-scale eddies, but are dominated by friction with the ground; the stratification is stable ($\frac{dT}{dz} > \left(\frac{dT}{dz}\right)_{ad}$). This happens normally during night time and low winds and leads to a thin boundary layer. In case of $\frac{dT}{dz} > 0$ temperature *inversion* occurs, making the atmosphere even more stable.

- *neutral*: if the air rising from the surface is in thermal equilibrium with the surrounding air, the stratification is said to be neutral ($\frac{dT}{dz} = \left(\frac{dT}{dz}\right)_{ad}$). This happens often in case of strong winds and late in the afternoon. Due to the strong winds this is often the most important situation to consider, but it is also often used because it is an 'average condition', in between stable and unstable conditions.

The (gradient) Richardson number is often used to indicate stability:

$$\text{Ri} = \frac{g}{T_0} \frac{\frac{dT}{dz}}{(\frac{dU}{dz})^2}, \tag{5}$$

with g the gravitational acceleration, T_0 a reference temperature, T the mean potential temperature and z the height above ground. The Richardson number can be interpreted as the ratio between thermally created turbulence (due to buoyancy) and mechanically created turbulence (due to velocity shear). The neutral stratification point is in theory $\text{Ri} = 0$, but this value is sometimes relaxed. Magnusson and Smedman [43] used for example:

- $\text{Ri} < -0.05$: unstable stratification (daytime condition with high insulation)

- $-0.05 < \text{Ri} < 0.05$: neutral stratification (overcast with high winds)

- $\text{Ri} > 0.05$: stable stratification (night or winter condition)

For $\text{Ri} > 0.25$ the atmosphere is considered not to be fully turbulent anymore.

Connected to the Richardson number is the Monin-Obukhov length, the height above the ground where mechanically and thermally created turbulence are in balance. It is often defined as (there seems to be some controversy in literature)

$$L = \frac{T_0 u^{*2}}{\kappa g T^*}, \tag{6}$$

where T^* is a temperature difference. $L > 0$ indicates stable conditions, $L < 0$ unstable conditions and $L = \infty$ applies to neutral conditions.

2.1.3 Turbulence

Atmospheric turbulence is known to be anisotropic [1] and is a function of surface roughness (section 2.1.1), atmospheric stability (section 2.1.2) and distance above the ground. Turbulence intensity is defined by

$$I = \frac{\sigma}{\bar{u}}, \tag{7}$$

where σ is the standard deviation of the wind velocity in the average wind direction, and $\bar{u}$ is the magnitude of the average wind velocity. In principle the intensity is different for each wind direction, from which the definitions for I_u, I_v and I_w follow. A known expression for σ_u is $\sigma_u \approx 2.5u^*$, which complies with the fact that turbulence intensity decreases with height (inside the ABL).

A well-known analytical model for atmospheric turbulence is the one of Panofsky and Dutton [56], often used in wind turbine simulations. Other models, from Veers, Mann, Bechmann will be discussed in section 4.2.6.

The energy spectrum of a turbulent velocity field should be, for large Reynolds numbers, proportional to $f^{-5/3}$ (in the inertial subrange), with f the frequency. Two expressions for the spectral density of the longitudinal component, S_u, are used: the Kaimal spectrum and the von Kármán spectrum. These expressions depend on σ_u and on length scales that typically depend on surface roughness and height above the ground.

2.2 Actuator disk concept

In this section we will use the classical actuator disk theory to describe the working of a wind turbine and to get a feeling for the physics of the flow field.

2.2.1 One-dimensional theory

Since a wind turbine extracts energy from the wind, a fluid element passing through the rotor disk loses part of its kinetic energy. The flow through a wind turbine slows down gradually from some upstream value u_∞ to an average value far downstream in the wake u_w. The static pressure increases from its upstream value p_∞ to a value p_d^+ just in front of the disk and then drops suddenly to p_d^- behind the disk, associated to the axial force exerted by the disk. The pressure gradually recovers in the wake to the freestream value p_∞, see figure 1.

Using this process of energy extraction by the actuator disk as a black box, a number of analytical relations can be derived using the equations of conservation of mass, momentum and energy (for incompressible flow):

$$\text{continuity:} \quad \dot{m} = \rho A_\infty u_\infty = \rho A_d u_d = \rho A_w u_w, \tag{8}$$

$$\text{force on disk:} \quad T = \dot{m}(u_\infty - u_w) = (p_d^+ - p_d^-)A_d, \tag{9}$$

$$\text{energy extracted:} \quad E = \frac{1}{2}m(u_\infty^2 - u_w^2). \tag{10}$$

The energy extracted per unit time gives the power, $P = \frac{1}{2}\dot{m}(u_\infty^2 - u_w^2)$. This power is equal to the power performed by the force T acting on the disk, $P = Tu_d = \dot{m}(u_\infty - u_w)u_d$. Equating these two expressions leads to:

$$u_d = \frac{1}{2}(u_\infty + u_w). \tag{11}$$

---

[1]isotropic turbulence: turbulence having statistical properties that are independent of direction
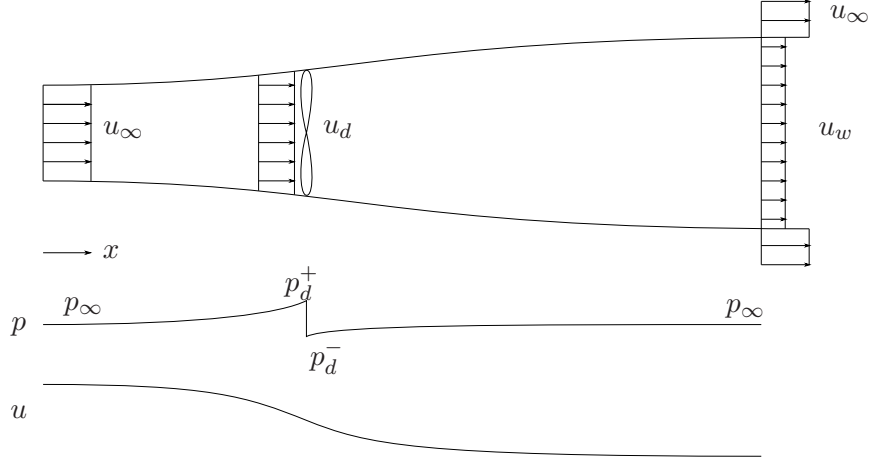
Figure 1: 1D flow through an actuator disk.

In order to compare the power of different wind turbines the power coefficient C_P is used, defined by:

$$C_P = \frac{P}{P_0} = \frac{P}{\frac{1}{2}\rho u_\infty^3 A_d},$$ (12)

i.e. the power is non-dimensionalized by the wind speed and the rotor swept area. The expression for the power coefficient becomes

$$\begin{aligned} C_P &= \frac{1}{2}(u_\infty + u_w)(u_\infty^2 - u_w^2)/u_\infty^3 \\ &= \frac{1}{2}(1+b)(1-b^2) = 4a(1-a)^2, \end{aligned}$$ (13)

where $a = 1 - \frac{u_d}{u_\infty}$ is the axial induction factor (often used in literature) and $b = \frac{u_w}{u_\infty}$, hence $a = (1-b)/2$. The optimal C_P is found at $a = b = \frac{1}{3}$, such that $C_{P_{\max}} = \frac{16}{27} \approx 0.59$, known as the *Betz limit*. It shows that, within the assumptions of the derivation, a maximum of 59% of the wind energy can be converted into mechanical power. A similar definition exists for the thrust coefficient C_T,

$$\begin{aligned} C_T &= \frac{T}{\frac{1}{2}\rho u_\infty^2 A_d} \\ &= 1 - b^2 = 4a(1-a). \end{aligned}$$ (14)

At optimal C_P the C_T is equal to $\frac{8}{9}$. Note that, due to the decrease in velocity behind the turbine, $u_w < u_d$, so that $A_w > A_d$; the wake expands. The higher C_T, the larger the wake expansion. In the wake the pressure gradually recovers from p_d^- to the ambient pressure p_∞ (note that $p_d^+ - p_\infty > p_\infty - p_d^-$!). The pressure difference between the near wake and the fluid 'outside' is supported by the centrifugal force due to the curvature of the streamlines.

The development of the velocity in the wake can be found by considering an inviscid vortex system [48]:

$$u_i/u_\infty = 1 - \frac{1-b}{2}\left(1 + \frac{2x}{\sqrt{1+4x^2}}\right),$$ (15)

with x the non-dimensional distance from the rotor disk and u_i the velocity in the wake. By expressing b in terms of C_T according to equation (14),

$$b = \sqrt{1 - C_T},$$ (16)
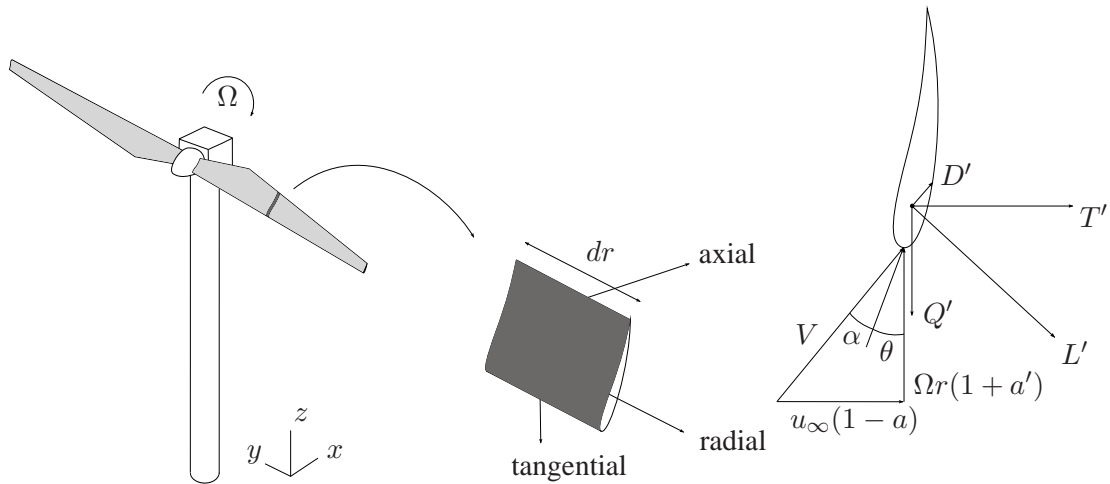
Figure 2: Nomenclature of wind turbine.

an expression for the velocity in the wake as a function of x and the thrust coefficient remains. The resulting curves of u_i versus x are shown for different C_T in figure 3. It can be seen that according to this inviscid 1D model the velocity is already close to u_w at two diameters downstream of the disk. In principle this velocity can be used to calculate the power production of a next actuator disk standing in the wake. However, one needs to decide which velocity to take for non-dimensionalizing the power and the thrust. Furthermore the thrust coefficient of the second turbine is not known.
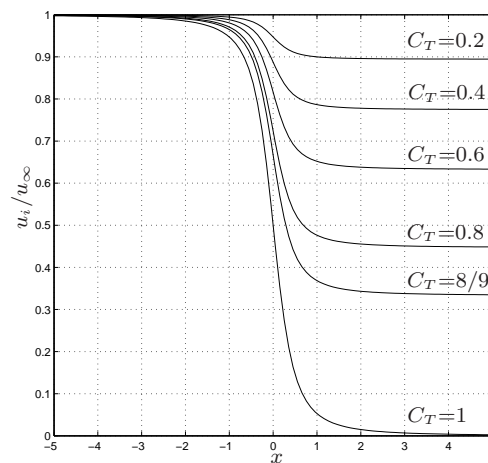
Figure 3: Velocity in the wake for some values of the thrust coefficient.

2.2.2 Rotational effects

In the foregoing analysis the shape of the energy converter was not taken into account. In practice the energy converter often consists of a number of turbine blades, which convert wind energy into rotational energy. The torque on the turbine blade is exerted by the flow passing over it. A reaction torque acts on the flow, causing it to rotate in the direction *opposite* to the rotor (counter clockwise when looking at the rotor). This means that a tangential velocity component is present in the wake, which is neglected in the actuator disk theory.
Looking at figure 2 one can distinguish the different velocity components that result in the velocity

V experienced by a small section of a blade. First, there is the axial component u_d, which is equal to $u_\infty(1-a)$ according to the definition of a. Secondly, the blades rotate with an angular velocity Ω, leading to a tangential component Ωr. Thirdly, there is a tangential velocity component u_t due to the reaction torque acting on the flow. By defining a tangential flow induction factor $a' = u_t/\Omega r$, the total tangential velocity component (also called azimuthal velocity) can be expressed as $\Omega r(1 + a')$. The total velocity V is therefore

$$V = \sqrt{(u_\infty(1-a))^2 + (\Omega r(1+a'))^2}, \tag{17}$$

with an angle ϕ to the freestream:

$$\tan\phi = \frac{u_\infty(1-a)}{\Omega r(1+a')}. \tag{18}$$

The angle of attack α follows from $\alpha = \phi - \theta$, where θ is the pitch angle of the blades. At the root, where r is almost zero, ϕ is almost $90°$ and blades are normally twisted here considerably to limit the local angle of attack.

The ratio of the tangential velocity of the tip of the blade to the freestream velocity is called the tip speed ratio:

$$\lambda = \frac{\Omega R}{u_\infty}. \tag{19}$$

Figure 2 also shows the definition of the forces that act on the blade. The sectional drag D' is by definition parallel to the flow vector $\vec{V}$, and the lift L' perpendicular to it. For a well designed airfoil L'/D' can be $\mathcal{O}(10^2)$. Alternatively one can decompose the force that acts on the blade in axial and tangential direction: the thrust T', and the torque Q' (both in Newton), respectively:

$$\begin{aligned} T' &= L'\cos\phi + D'\sin\phi, \\ Q' &= L'\sin\phi - D'\cos\phi. \end{aligned} \tag{20}$$

2.3 Vorticity-based description of the flow field

To gain a deeper understanding of the flow behind a wind turbine it is convenient to use the concept of vorticity, because the velocity field follows once the vorticity distribution is known.

The lift force generated by the blades can be attributed to a distributed *bound vortex* (total strength $\Delta\Gamma$) via the Kutta-Joukowski law: $L = \rho V \Delta\Gamma$. The bound vortex is responsible for the jump in tangential velocity over the blade and as such the pressure difference and the lift.

At the tip of the blade, the difference in pressure between the lower and upper side leads to the formation of a *tip vortex*. This tip vortex first decreases in diameter (vortex stretching due to wake expansion), and then increases in diameter due to viscous effects [82].
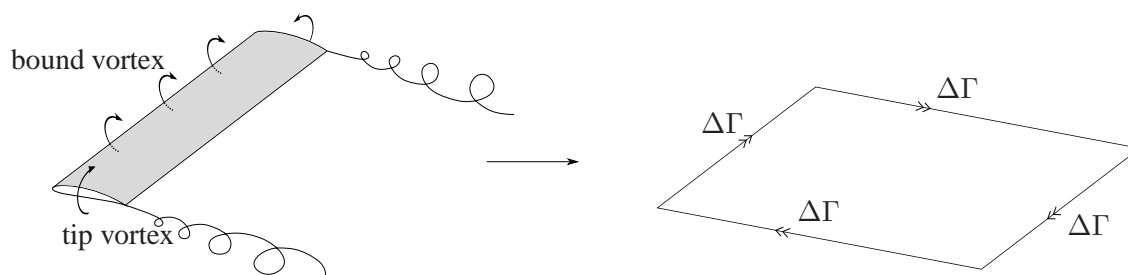
Figure 4: Vortex system on finite wing.

To evaluate the vortex system of a wind turbine, it is useful to first consider a stationary finite

wing. The bound vortex and tip vortices form a horseshoe vortex, see figure 4. For an inviscid, incompressible flow Kelvin's theorem states that $\frac{D\Gamma}{Dt} = 0$, where Γ is the circulation. The circulation of the bound vortex on the wing therefore has an equal and opposite vortex far downstream. This starting vortex, which was formed when the flow over the wing started, closes the horseshoe system far downstream. Similarly, the two tip vortices are of equal strength, but of opposite sign.

In case of a wind turbine, this vortex system is still present, but rotates. Figure 5 shows the direction of the bound, tip and root vortex. The root vortex at the hub is formed by the different 'tip' vortices and has strength $\Gamma = B\Delta\Gamma$, B the number of blades. The root vortex (and for small λ also the tip vortex) causes the tangential velocity at the blades; its rotation is opposite to that of the rotor. The tip vortices follow a helical path with rotation opposite to the rotor. For a large number of blades, the different tip vortices are close together, which leads to the concept of a tubular *vortex sheet*. Because the tip vortices have a tangential component, they induce an axial velocity at the blades, which causes the deceleration of the flow in front of the turbine. For large λ the path of the tip vortices will be almost parallel to the rotor plane; the angle of the helical path is given by the flow angle at the blade tip, ϕ, and is inversely proportional to λ.

3D view   top view
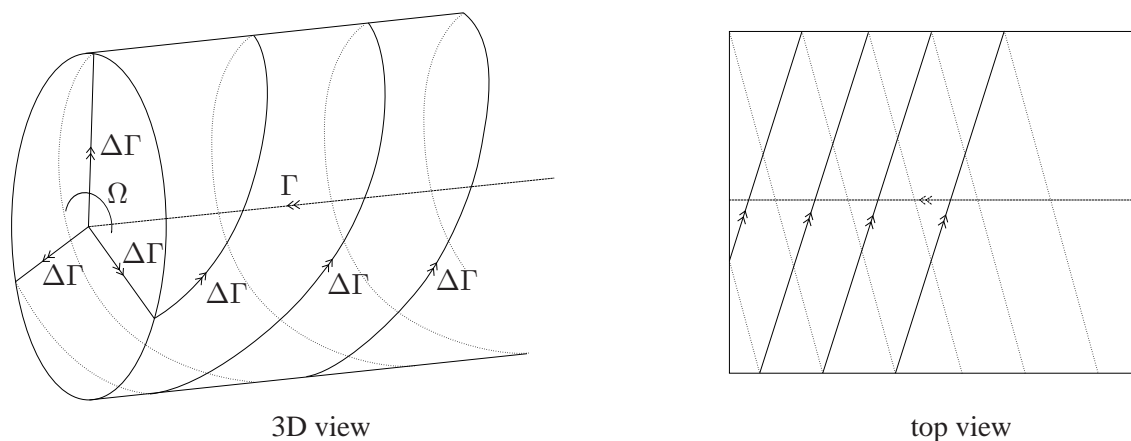
Figure 5: Vortex system on three-bladed rotating turbine.

In this model the vorticity is therefore confined to the surface of the tube, the root vortex and to the bound vortex sheet swept by the multiplicity of blades forming the rotor disk. Everywhere else the flow is irrotational. However, in general the model above is too simplified since it neglects the spanwise variation of bound vorticity, and the viscosity of the flow. Although this means that in reality vorticity is shed from the entire blade, the model presented above still gives a good indication of where most vorticity is concentrated.

2.4   Near and far wake; turbulence, velocity deficit and vorticity

The wake of a wind turbine is typically divided into a near and a far wake [81]. The former is the region from the turbine to approximately one rotor diameter downstream, where the turbine geometry determines the shape of the flow field, determining the performance of the turbine. The axial pressure gradient is important for the development of the wake deficit. The latter is the region in which the actual rotor shape is less important, but the focus lies on wake modeling, wake interference (wake farms), turbulence modeling and topographic effects.

In reality the vortex system and velocity profiles are not as ideal as presented in the sections above. The difference in velocity between the air inside and outside the wake results in a shear layer, which thickens when moving downstream. In the shear layer turbulent eddies are formed. Due to the ambient shear flow, the turbulence in the shear layer is non-uniform, i.e. the turbulence intensity in the upper part is larger than in the lower part. In the near wake this leads to two peaks in the turbulence intensity, but in the far wake they are no longer discernible. Figure 6 gives

a more realistic picture of the velocity profile in the wake (compared to figure 1). Ainslie [2] estimates that the maximum velocity deficit is attained after 1-2 rotor diameters (D), but for low ambient turbulence levels this might be longer. The expansion region length is also about 1 D [16]. Based on the best comparison with experiments, Schepers uses 2.25 D as the distance where the wake is fully expanded [59].
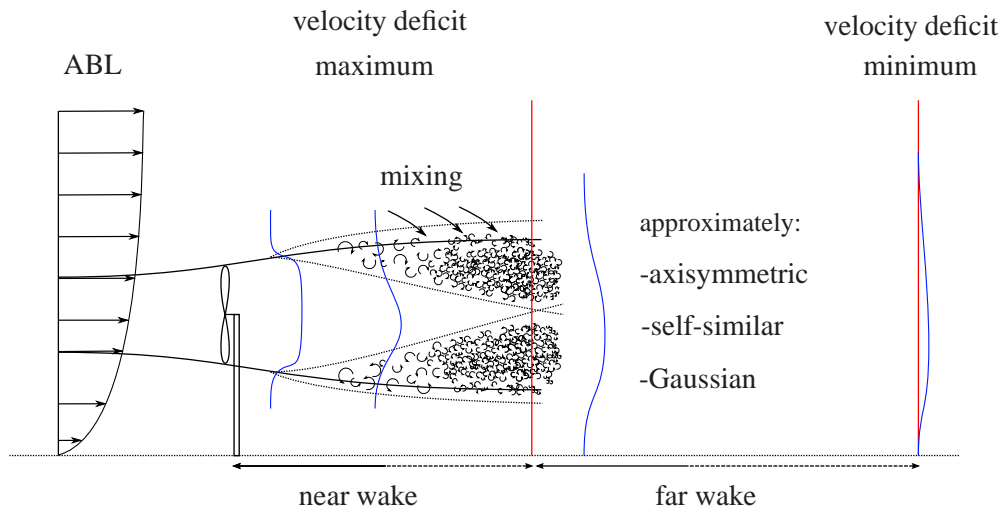
Figure 6: Velocity profile in the wake of a wind turbine.

The higher the thrust on the rotor, the lower the wake velocity u_w and the larger the shear, i.e. the difference between flow velocities inside and outside of the wake. For very high rotor loading a considerable amount of kinetic energy of the incoming flow is converted into large-scale turbulent motion, leading to the *turbulent wake state* (typically $a > 0.5$). The turbulence in the wake is an efficient mixer: it mixes the low velocity fluid in the wake with the high velocity fluid outside it. In this way momentum is transferred into the wake; the wake expands, but the velocity deficit is reduced. The growth of the turbulent wake depends on [40]: (i) turbulence levels in the atmosphere, (ii) surface constraint effects, (iii) wind shear effects (vertical wind gradients), (iv) topographic and structural effects. Lower ambient turbulence levels (stable stratification) typically lead to larger wake velocity deficits and to longer distances over which the wake recovers. The turbine power deficit (the power difference between the current turbine and the first turbine in the row) is therefore maximal at high thrust settings (low wind speed) and low ambient turbulence level [22].

Other sources of turbulence are formed by the tip vortices, turbulent boundary layers leaving the blades, the presence of the nacelle and tower ('mechanical turbulence') and of course turbulence in the atmosphere. The mechanical turbulence is of high frequency and decays relatively quickly. The tip vortices, which are present in the shear layer, will have been broken down after approximately 4 D [1, 2]. When the shear layer becomes so thick that it reaches the wake axis, the end of the near-wake has been reached (2-5 D) [16].

After this, pressure gradients are less important and the velocity deficit gradually decays, depending strongly on turbulence levels in the wake. In the far wake, the wake is completely developed; when making a number of assumptions such as axisymmetry, $\frac{\partial p}{\partial x} = 0$ and $\frac{\partial^2 u}{\partial x^2} = 0$, it can be found that self-similar solutions (Gaussian profiles) for the velocity deficit and turbulence intensity exist [1, 60]. However, due to the presence of the ground and the shear of the ambient flow this is not completely valid. In reality it is observed that the point of maximum velocity deficit is below the turbine axis (which is attributed to the tower shadow) and the point of maximum turbulence intensity above it (because velocity shear is larger there, except in a very stable atmosphere). These effects are illustrated in figure 7. Ammara et al. [3] mention that experimental and theoretical studies have suggested that the wake velocity deficit is minimal after 10 D (where

they probably mean that the velocity deficit is smaller than a certain percentage of the free stream velocity). Indeed it is common practice to space wind turbines 6-10 D in the predominant direction. In crosswind direction the spacing is 1.5-3 D. For large wind turbines (D around 100m) this leads to sparse wind farms, which are costly (especially on-shore, but also off-shore).

The decay of the velocity deficit is more rapid than the decay of turbulence intensity; Højstrup [27] mentions that the mechanical turbulence in the wake is still 'noticeable' after 15 D. The turbulence leads to higher loading; Dahlberg [18] showed that for the Alsvik wind farm (Sweden) in case of full-wake conditions the loads increased by 10% at 9.5 D and to 45% at 5 D. Measurements on the Vindeby farm in Denmark showed a significant fatigue loading increase of 80% when two turbines were aligned with the wind. However, the difference in loading for single and multiple wake conditions is small. At sea, with low roughness and low ambient turbulence levels, wake effects can be very important.

The turbulence in the wake and in the outer ambient flow is anisotropic. However, the turbulence in the wake is more isotropic than in the outside flow, especially in the center of the wake. Not surprisingly, peaks in turbulence intensity are observed in the shear layer, see figure 7a.
The turbulence energy spectrum shifts towards higher frequencies (in agreement with the breakup of turbulent eddies), and the turbulence in the wake exhibits much smaller length scales than freestream turbulence. For low frequencies there may be a decrease in turbulence, because the wind turbine extracts energy from the wind in the low frequency range.

In case of shear flow and a cross wind velocity component Zahle and Sørensen [90] show that the wake is largely disintegrated after already 3 D, due to upward ejection and mixing of the low velocity fluid near the ground with higher velocity near the upper part of the wake.

(a) Turbulent velocity [64]   (b) Velocity deficit [81]
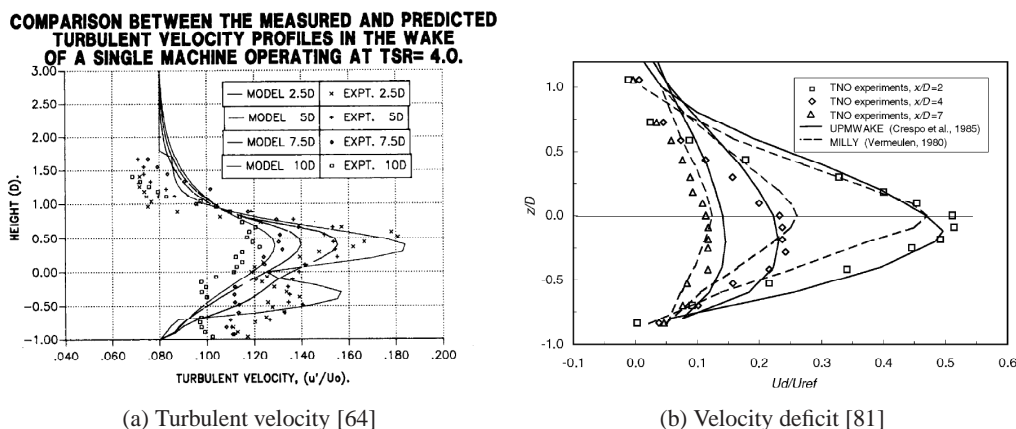
Figure 7: Turbulence and velocity deficit in the wake at various downstream distances.

2.5   Wind farm aerodynamics

As mentioned before, the placement of wind turbines in a park leads to power losses and increased loading. Lissaman [39] showed the two most important factors influencing array efficiency (i.e. the generated power of the total wind farm divided by the total power that could be generated by the same amount of wind turbines if standing isolated): *field geometry* and *ambient turbulence intensity*. The influence of field geometry, i.e. the way in which turbines are placed, is obvious. The influence of the ambient turbulence is twofold. High ambient turbulence levels lead to turbulent mixing in the wake and the faster the velocity field recovers. For off-shore wind farms the ambient turbulence is often lower than on-shore, leading to more persistent wakes. Other factors that influence the array efficiency are: the terrain lay-out, the wind-frequency distribution (wind rose) and the operating settings of the turbines (e.g. thrust coefficient). For example, array losses

decrease with increasing wind speed [22]: wake effects diminish because the thrust coefficient decreases. These parameters are very much the same as the parameters influencing the growth of the turbulent wake, mentioned in section 2.4.

Apart from the ambient turbulence, the mechanical turbulence created by the turbine is important. In general, a higher turbulence level in the wake leads to larger loads for downstream turbines. However, it has also been found that for some turbines the loads were smaller [41]. In this study it was also found that the highest loads on a downstream turbine occur when a rotor is only partially immersed in the wake of an upstream turbine.

The wake of a downstream turbine recovers more quickly than the one upstream, due to the increased turbulence levels generated by the upstream turbine which leads to better turbulent mixing in the downstream wake ('entrainment'). The incremental energy loss between turbines decreases the farther the turbines are located from the first turbine. The second turbine experiences a significant decrease in power, but the loss in successive machines is much smaller. The rate of decrease of wind velocity tends to reach an equilibrium value. A possible explanation for the approximately constant power for downstream turbines is that after several rows of turbines the turbulence is saturated and an equilibrium value is reached. This trend is visible in figure 8, taken from the UPWIND project [4]. Both the experiments and numerical models show that in case of inflow aligned with the turbine row ($2.5°$ sector) the loss in relative power is quite dramatic.
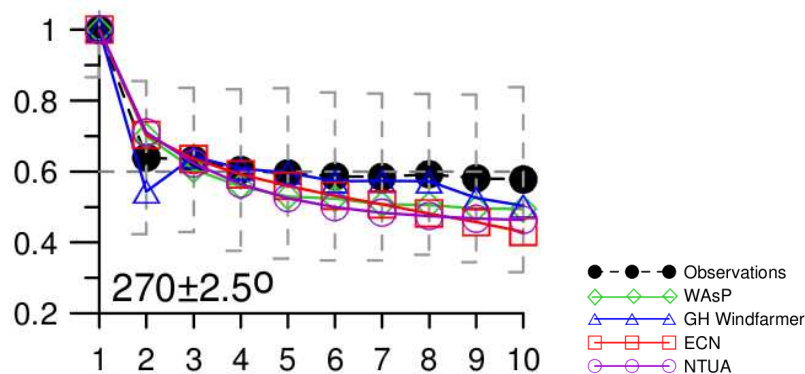
Figure 8: Power (normalised) as function of turbine number in a wind farm at a wind speed of 8 m/s; different models compared to measurements [4].

2.6 Wake meandering

Wake meandering is the term used for the large scale movement of the entire wake, see for example figure 9. It is thought to be due to eddies that are large in comparison with the size of the wake (large scale atmospheric structures). Wake meandering is important because it might considerably increase extreme loads and fatigue loads and in particular yaw loads on turbines in wind farms, because the meandering causes the wake to be swept in and out of the rotor plane of downstream turbines. On the other hand, the meandering helps to reduce the mean wake deficit and therefore alleviates power losses.

Ainslie [2] was the first to model the effect of wake meandering on wake deficits by relating wake meandering to the variability in wind direction. He assumes that the large eddies increase linearly in size with x and in proportion to the standard deviation of the wind direction. He finds that the influence of meandering is significant in reducing the depth of the deficits. Larsen et al. [36] study wake meandering extensively, both with a numerical model and with experiments (see section 4.2.3 for more information on the numerical aspects). The experiments are done with LiDAR measurements of a full-scale wake. They conjecture that the transport of the wake can be modeled as if it acts as a passive tracer driven by the large-scale turbulence structures in the

ABL. The meandering of the wake leads to the concept of 'apparent' turbulence intensity, i.e. the normal turbulence present in a wind turbine wake plus velocity components due to the movement of the wake, which would not be present in a meandering frame of reference.
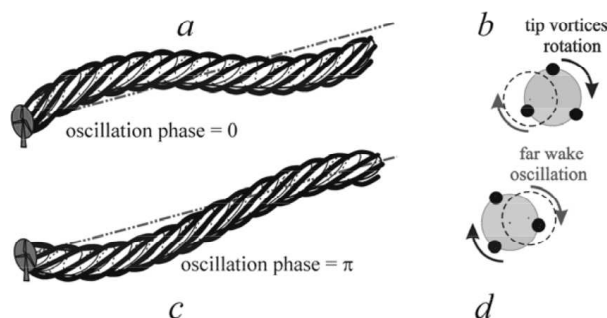
Figure 9: Wake meandering according to [36].

Medici and others found strong evidence in experimental studies that wake meandering is caused by an instability of the wake, similar to large-scale coherent structures behind bluff bodies [49], [50]. This low-frequency fluctuation was found both with and without free stream turbulence and was stronger in case of yawed inflow. Analogously to bluff body flows, a Strouhal number for wake meandering was defined, St $= fD/u_\infty$, and for high λ it was found to be close to the Strouhal number of a solid circular disk. A clear dependence on λ, C_T, number of blades and pitch angle was found, and regions in the $C_T - \lambda$ plane were identified for which no meandering occurred. Although the experiments were done in a wind tunnel at a lower Reynolds number than of a real turbine, this opens opportunities for controlling wind turbine wakes.

2.7 Effect of yaw

Due to the variability in wind direction a wind turbine is usually facing the wind under a yaw angle γ. Yawed inflow leads to a lower efficiency and to a periodic variation in the angle of attack on the blades and therefore to fatigue. The angle of the wake with the rotor axis, χ, is larger than γ. The resulting skewed wake is not symmetric with the turbine axis. Skewed wakes have the downwind side of the rotor closer to the wake centerline than the upwind side of the rotor. Medici [49] shows that a yawed turbine deflects the wake to the side, showing the potential of controlling the wake position by yawing the turbine. This concept, Controlling Wind, is investigated at ECN to increase the power output of a wind farm.
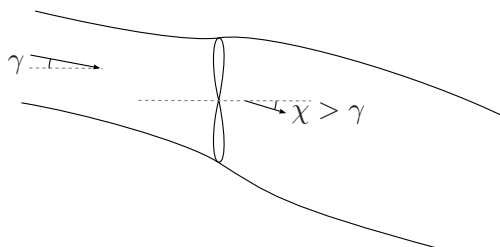
Figure 10: Yawed inflow with wake turned away from centerline.

3 Engineering models

This chapter deals with the 'engineering' models used in wind turbine design, methods that are not directly based on the physical principles of conservation of mass, momentum and energy. The blade element method is treated quite extensively, because it is widely in use as blade design tool, and more importantly for this review, it is used frequently in many CFD codes (the actuator-type methods to be discussed in chapter 4).

3.1 Blade element momentum method

3.1.1 Principles

In the blade element momentum method (BEM) the blade is split in small elements (see figure 2). The performance of the turbine can be calculated by summing the contribution of all these elements. This method is still the basis for many rotor design codes. For each element the forces L' and D' are obtained from two-dimensional tabular airfoil data. In tables the non-dimensional lift and drag coefficients c_l and c_d are given, from which the lift and drag follow:

$$
\begin{aligned}
L' &= c_l \frac{1}{2}\rho V^2 c, \\
D' &= c_d \frac{1}{2}\rho V^2 c,
\end{aligned}
\tag{21}
$$

where c is the local chord. Note that c_l, c_d, V and c are a function of r. Expanding the expression for thrust and torque and using that $V = u_\infty(1-a)/\sin\phi = \Omega r(1+a')/\cos\phi$ (this is useful for the next step):

$$
\begin{aligned}
dT = BT'dr \quad &\rightarrow \quad dT = \frac{1}{2}\rho B \left(\frac{u_\infty(1-a)}{\sin\phi}\right)^2 c\, c_t\, dr, \\
dQ = BrQ'dr \quad &\rightarrow \quad dQ = \frac{1}{2}\rho B \left(\frac{u_\infty(1-a)}{\sin\phi}\right)\left(\frac{\Omega r(1+a')}{\cos\phi}\right) c\, c_q\, r\, dr.
\end{aligned}
\tag{22}
$$

where B is the number of blades, $c_p = (c_l\cos\phi + c_d\sin\phi)$ and $c_q = (c_l\sin\phi - c_d\cos\phi)$. These expressions are put in this form because they will be equalized to the thrust and torque expressions from momentum balance considerations:

$$
\begin{aligned}
dT = (u_\infty - u_w)d\dot{m} &= 2\pi r\rho u_d(u_\infty - u_w)\, dr \\
&= 4\pi r\rho u_\infty^2(1-a)a\, dr.
\end{aligned}
\tag{23}
$$

$$
\begin{aligned}
dQ = ru_{t,w}d\dot{m} &= r2\pi r\rho u_d 2a'\Omega r\, dr \\
&= 4\pi r^3\rho u_\infty\Omega(1-a)a'\, dr.
\end{aligned}
\tag{24}
$$

In deriving these equations we have used that $u_\infty - u_w = 2a$ and that $u_t = \frac{1}{2}(u_{t,\infty} + u_{t,w}) = \frac{1}{2}u_{t,w}$, so $u_{t,w} = 2a'\Omega r$. In this way expressions can be found for a and a':

$$
\begin{aligned}
a(r) &= \frac{1}{\frac{4\sin^2\phi}{\sigma c_t} + 1}, \\
a'(r) &= \frac{1}{\frac{4\sin\phi\cos\phi}{\sigma c_q} - 1},
\end{aligned}
\tag{25}
$$

with the (chord) solidity σ defined as

$$\sigma(r) = \frac{cB}{2\pi r}. \tag{26}$$

These expressions for the axial and tangential flow induction factor are useful, because they can be used in an iterative scheme:

1. Start with estimated values for a and a', e.g. $a = a' = 0$.

2. With given values for u_∞ and Ω (or λ), calculate $\phi(r)$ with (18).

3. Given the pitch setting of the blade, find the local angle of attack, $\alpha(r) = \phi - \theta$.

4. Find the values of c_l and c_d as function of α, either from measurement data or computations.

5. Compute $c_t = c_l \cos \phi + c_d \sin \phi$ and $c_q = c_l \sin \phi - c_d \cos \phi$.

6. Update a and a' according to equations (25). If not converged, go back to step 2.

Other iterative schemes are also possible and are in use as well. Finally, the power coefficient can be found as (in non-dimensional parameters):

$$C_P = \frac{P}{\frac{1}{2}\rho u_\infty^3 A_d} = \frac{B\lambda}{\pi} \int_0^1 c_q(\bar{r}) \left[(1-a)^2 + (\lambda \bar{r})^2 (1+a')^2\right] \bar{c}(\bar{r}) \bar{r} \, d\bar{r}, \tag{27}$$

with $\bar{c} = c/R$ and $\bar{r} = r/R$. We have used that $P = \frac{\int_0^R \Omega \, dQ}{\frac{1}{2}\rho u_\infty^3 A_d}$ and $A_d = \pi R^2$.

An example of the behavior of the power coefficient as function of λ calculated by the BEM is shown in figure 11, taken from [10]. A two-blade rotor with NACA632xx airfoil profile and varying thickness along the span was used as input. Such a computation can be easily performed on a desktop computer by using the iterative scheme shown above, as long as accurate airfoil data are available.
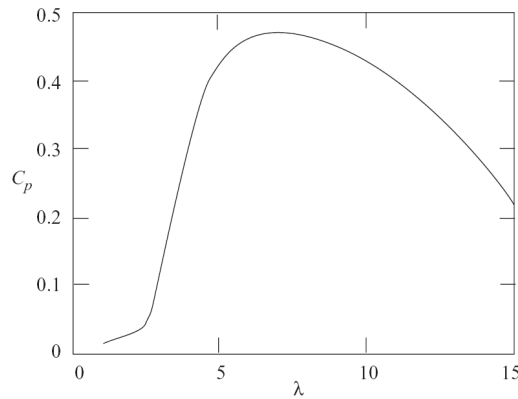
Figure 11: Typical behavior of the power coefficient versus tip speed ratio [10].

3.1.2   Improvements and limitations

Here we list the most important limitations and improvements of the BEM, for a more elaborate discussion see the review of Snel [65].

- In the BEM it is assumed that the force by the blades on the flow is constant on an annular element of the rotor disk, see equation (23). This corresponds to an infinite number of blades. In reality the number of blades is finite, leading to a tip loss. A correction factor ('Prandtl's tip loss factor') is usually applied. Furthermore, the different annular rings are assumed to be independent, which is not correct and completely inadequate in case of yaw misalignment. Improvements have been made and now give reasonable comparison with measurements.

- For heavily loaded rotors ($a > 0.4$) the actuator disk approach breaks down. The velocity difference between the wake (u_w is almost zero) and the freestream becomes so large that the shear layer becomes unstable and a turbulent wake develops. Glauert developed, amongst others, an empirical correction for the thrust coefficient.

- The BEM assumes an equilibrium between the difference in momentum far upstream and far downstream and the forces acting on the rotor blades, which is only valid when the flowfield is steady. In practice the dynamic nature of the inflow makes the flowfield unsteady, and this has been taken into account in most modern design codes.

- Furthermore, in calculating the sectional lift and drag with a boundary layer code, it is necessary to take into account fictitious forces (like Coriolis) due to the rotation of the blades (see section 4.2.1).

Still, after applying these corrections, it will be hard (if not impossible) to model atmospheric turbulence, wind shear due to ground effect, deep stall, the effect of neighboring turbines and so on [81].

3.2   Lifting line method and vortex wake method

Lifting line and vortex wake methods are based on the assumption of incompressible, inviscid flow. The presence of a discrete number of vortex lines leads to a velocity field, following the Biot-Savart law.

In lifting line methods the turbine blades are represented by bound vortex lines, similar to section 2.3. The vortex strength depends on the lift coefficient, $\Gamma = \frac{1}{2} c_l \, c \, V$, which is obtained from tabulated data, like in the BEM. The sectional (profile) drag c_d is not included in the method, and only induced drag, a 3D effect, can be calculated. In the more advanced lifting surface methods (also known as vortex lattice methods), the geometry of the blades is better represented by discretizing the surface with patches, or vortex elements, instead of using a single line.

According to Kelvin's theorem, vorticity is shed from the trailing edge into the wake. In the vortex wake method, the vorticity in the wake is modeled by a distribution of vortex singularities, see for example [79]. Note that if the spanwise variation of bound vorticity is neglected, vorticity is only shed from the tip and the root of the blade, like in figure 5.

The advantage of the vortex wake method is that it does not rely on the global momentum balance, as the BEM method does. This offers the ability to calculate unsteady conditions and to handle yaw misalignment, which can be used for example as correction for BEM models. The disadvantage is that the Biot-Savart kernel (Green's function) has to be regularized to prevent singular behavior when vortex lines or collocation points are close to each other (so-called cut-off functions). Another disadvantage is the large amount of CPU time necessary in the case of free-wake calculations (i.e. the wake position is part of the solution). Prescribing the wake decreases computational time significantly, but the results are less accurate.

3.3 Boundary integral equation method

The boundary integral equation method uses the fact that for incompressible, inviscid, irrotational flow it is possible to set up a velocity potential $\vec{u} = \nabla\phi$, satisfying $\nabla^2\phi = 0$. Using Green's identity this can be transformed into a solution for ϕ in terms of surface integrals only (therefore 'boundary integral' method). The actual surface geometry is discretized in panels consisting of singularities, which are Green's functions of the Laplace equation. The method is therefore also known as *panel method*. Viscous effects can be taken into account by superposing an (integral) boundary layer (viscous-inviscid interaction).

The advantage of this method is that it takes into account the exact geometry of the blades without the need to discretize the entire flow field. However, accurately calculating turbulent boundary layers and separated flow remains very difficult. Furthermore, in order to correctly calculate lift it is necessary to introduce a singularity distribution in the wake.

3.4 Wind farm and wake models

Material in this section comes primarily from the survey of Crespo, Hernández and Frandsen [16] and the review of Vermeer, Sørensen and Crespo [81].

The simplest expressions describing the wake are the engineering expressions, which give an estimate of the order of magnitude of the most important parameters influencing wake evolution: the velocity deficit and the turbulence intensity. For the velocity deficit a power law is usually of the type

$$\frac{\Delta V}{V_{hub}} = A \left(\frac{R}{x}\right)^n , \tag{28}$$

with R the turbine radius, A a constant depending mostly on the thrust coefficient C_T and n depending on the type of the wake (e.g. laminar/turbulent). The turbulence intensity ΔI due to the wake is added to the ambient turbulence, $I^2 = \Delta I^2 + I_\infty^2$, based on the addition of kinetic energy. For ΔI different expressions have been obtained by fitting experimental and numerical data, see e.g. [81] and [10], which depend primarily on C_T, x and I_∞. As mentioned before, the increase in turbulence intensity is noticeable further downstream than the deficit in the velocity field. Although good agreement has been obtained with certain experiments, the validity of these engineering expressions have not been checked in more general situations.

The first models for modeling the effect of wind turbines in wind farms were made by considering the turbines as distributed roughness elements. The surface roughness of the logarithmic profile, equation (1), is increased to take into account the presence of the turbines. This concept has been used in the 1970s by several authors, but is hardly used nowadays [16]. A possible application for which this approach might still be useful is the influence of a park on the local atmosphere and park-park interaction. An overview of methods is given by Bossanyi [9].

A more accurate approach is to consider each turbine individually. One of the first investigations was by Lissaman, who used self-similar velocity deficit in the wake (mentioned in section 2.4) to predict the influence of wind turbines on each other [39]. He used linear superposition of the perturbations created by the wakes. This research formed the basis for the so-called *kinematic models*, which are still widely in use. Velocity profiles can be based on models for co-flowing jets; the thrust coefficient determines the initial velocity deficit. Wake growth is then (for example) assumed to be linear with distance. Vermeulen, for example, used a Gaussian profile and included effects of turbulence on the wake growth in his program MILLY [83]. With the assumption of axisymmetry, Crespo et al. [15] find for the velocity deficit a decay with $x^{-2/3}$ and for the turbulence intensity $x^{-1/3}$. Taking into account the ground effect remains a difficulty for the kinematic models, but still many results are in good agreement with experimental results (often after appropriate tuning).

With the advance of computers *field models* were also developed, based on the solution of the (simplified) Navier-Stokes equations. These models will be discussed in chapter 4.

4   Computational Fluid Dynamics

The engineering methods mentioned in the previous chapter serve for designing wind turbine blades and obtaining estimates of the wake. For calculating the near and especially the far wake accurately more sophisticated methods are necessary, methods that rely on the first principles of conservation of mass, momentum and energy. In this chapter we will first look at the partial differential equations governing fluid flows, the Navier-Stokes equations, and their properties relevant for wind turbine applications (section 4.1). Section 4.2 then discusses different modeling issues, most importantly being rotor modeling (section 4.2.2), wake modeling (section 4.2.3), and inflow modeling (section 4.2.6). Section 4.3 deals with the question how to verify and validate CFD codes.

4.1   Governing equations and their properties

4.1.1   Compressibility

The flow of air without heat sources is generally considered incompressible if the local Mach number does not exceed 0.3. In the standard atmosphere at sea level this corresponds to a flow velocity of approximately 100 m/s. Snel [66] mentions that the assumption of incompressibility is completely justifiable, although van der Pijl [78] mentions that when the rotor is modeled directly, compressible effects can occur at the blade tips. Indeed, current turbines reach tip speeds of 75 m/s, and the resulting maximum speed on the suction side can be higher than 100 m/s. However, the velocities in the wake remain much lower and for wind farm applications incompressibility is a valid assumption.

4.1.2   Viscosity, Reynolds number, turbulence and scales

The Navier-Stokes equations for such an incompressible flow read:

$$
\nabla \cdot \boldsymbol{u} = 0,
$$
$$
\frac{\partial \boldsymbol{u}}{\partial t} + (\boldsymbol{u} \cdot \nabla)\boldsymbol{u} = -\frac{1}{\rho}\nabla p + \nu \nabla^2 \boldsymbol{u}. \tag{29}
$$

When non-dimensionalizing this equation the Reynolds number Re appears as dimensionless parameter. In wind energy applications it is normally based on the chord and rotational speed at a certain radius along the blade, $\mathrm{Re} = \frac{\Omega r c}{\nu}$. Because the rotational speed increases and the chord decreases with increasing radius the Reynolds number may not vary much along the blade. For large turbines is is of the order $\mathcal{O}(10^6)$ or even higher. These high Reynolds numbers, combined with turbulent inflow, blade roughness and the presence of an adverse pressure gradient will certainly lead to turbulent flow over a wind turbine blade (although a laminar region can still exist).

The difficulty associated with turbulence is that turbulent flows exhibit much smaller scales than laminar flows, namely the scales at which energy dissipation takes place. The higher the Reynolds number, the finer these small-scale structures [19]. When denoting the scale of the smallest eddies by η, it can be found that $\eta \sim \mathrm{Re}^{-3/4}$; computing three-dimensional flows and resolving all scales (Direct Numerical Simulation) amounts to computations with a complexity per time step of the order $(1/\eta)^3 = \mathrm{Re}^{9/4}$. For all practical flow problems this is impossible, and therefore closure models have been constructed that represent the behavior of the small scales (RANS, LES).

In RANS (Reynolds Averaged Navier-Stokes) methods the turbulent fluctuations are averaged. Apart from the difficulty in finding an appropriate closure model and corresponding parameters

[2], the method does not do justice to the large-scale, low-frequency unsteadiness present in highly separated flows. Furthermore the Boussinesq hypothesis (an eddy-viscosity model used in e.g. $k-\epsilon$ and $k-\omega$) assumes that turbulent diffusion is isotropic, which is not the case for atmospheric flows. Crespo et al. adapted the constants of the $k-\epsilon$ model for atmospheric flow [17], but still $k-\epsilon$ models are too diffusive for wind energy applications. Lately El Kasmi and Masson [34] added an extra term to the transport equation for the turbulence energy dissipation rate, significantly improving agreement with experiments. Another model that gives better agreement with experiments is the Reynolds stress model (RSM), which does not use the eddy-viscosity approach but instead develops second-order closure relations. It is able to deal with anisotropic flow, but is more expensive and has rarely been used in wind energy applications.

In LES (Large Eddy Simulations) only the large eddies of the flow are calculated while the eddies smaller than the grid are modeled with a sub-grid scale model. This is based on the fact that the smallest eddies in the flow have a universal character that does not depend on the flow geometry. In the vicinity of walls the computational requirements for LES become extremely high and a coupling with RANS computations is often made (so-called DES - Detached Eddy Simulation).

Correctly simulating the Reynolds number is less important when the solid boundaries of the blades are not simulated directly, but are represented by an actuator disk or blade element method. It was shown by J.N. Sørensen [71] that the solution did not change noticeably when the Reynolds number was larger than 1000 (see also [66], [30], [70]). This corresponds roughly to results obtained by research on the nature of the interface between turbulent wakes and jets and the outer flow, which was found to change around Re $\sim 10^4$ [19]. Whale et al. [86] also found that the behavior of the wake may be rather insensitive for the blade Reynolds number.

4.1.3 Time dependency

The Navier-Stokes equations, (29), describe unsteady flows. In calculations of wind turbine wakes, especially with RANS models, steady flow is often assumed. However, a number of sources of unsteadiness are present in wind turbine flows:

- the rotation of the blades,

- the dynamic nature of the inflow (unsteady, turbulent),

- the stall of turbine blades (especially near the root), the deflection of the blades (aeroelastic effects), the tower shadow.

For wake computations especially the first two items are important, and therefore the unsteady term $\frac{\partial \boldsymbol{u}}{\partial t}$ should not be neglected.

4.1.4 Velocity-vorticity formulation

In flows dominated by vorticity, it can be advantageous to consider the Navier-Stokes equations in velocity-vorticity formulation, which are obtained by taking the curl of equation (29):

$$\frac{\partial \boldsymbol{\omega}}{\partial t} + (\boldsymbol{u} \cdot \nabla)\boldsymbol{\omega} = (\boldsymbol{\omega} \cdot \nabla)\boldsymbol{u} + \nu \nabla^2 \boldsymbol{\omega}, \tag{30}$$

where $\boldsymbol{\omega} = \nabla \times \boldsymbol{u}$. This formulation was for example used by Hansen [25], and the similar vorticity-streamfunction formulation was used by J.N. Sørensen [67, 69]. This formulation has a number of advantages [81]:

---

[2]George Gamow, 1999, on $k-\epsilon$: 'With five free parameters a theorist could fit the profile of an elephant'.

- Conservation of vorticity is an intrinsic property of the formulation, which is important in the simulation of vortex dominated flows.

- Non-inertial effects (for example Coriolis forces) arising from rotation and translation of the frame of reference are easily taken into account by taking $\boldsymbol{\omega}^* = \boldsymbol{\omega} + 2\boldsymbol{\Omega}$. Equation (30) then holds for $\boldsymbol{\omega}^*$ instead of $\boldsymbol{\omega}$.

- Since the pressure term has disappeared from the equations, the difficulty associated with pressure-velocity coupling is removed. The relation between the velocity and vorticity is linear.

However, there are a number of drawbacks:

- Either the Cauchy-Riemann equations ($\nabla \cdot \boldsymbol{u} = 0$ and $\nabla \times \boldsymbol{u} = \boldsymbol{\omega}$) need to be solved (which are overdetermined), or a Poisson equation has to be solved, in order to obtain the velocity from the vorticity.

- The boundary conditions for the vorticity are not as obvious as those for the velocity.

- The pressure is not part of the solution, but has to be obtained in a post-processing step.

Lastly, numerical schemes and turbulence models have been less developed for vorticity formulations. These form probably the reasons that in recent years most simulations of wind turbine wakes are done with the primitive variable (u, v, p) approach.

4.2 Modeling techniques

4.2.1 Choice of reference frame

Rotor-fixed. A rotor-fixed reference frame is primarily suitable when only a single, isolated rotor is considered. It facilitates the mesh generation because the mesh is not required to move, however, additional terms (fictitious forces) have to be added due to the rotation of the rotor-fixed frame with respect to an inertial reference frame fixed at the hub.

Consider a fluid element with mass m and acceleration a_{rel}, 'rel' meaning relative to a local reference frame. In an inertial reference frame Newton's second law would read $\boldsymbol{F} = m\boldsymbol{a}$, but because the local reference frame turns with an angular speed $\boldsymbol{\omega}$ and moves with acceleration $\boldsymbol{a}$ with respect to the inertial reference frame, Newton's second law in a non-inertial reference frame becomes:

$$m\boldsymbol{a}_{\text{rel}} = \boldsymbol{F} - m\boldsymbol{a} - m\dot{\boldsymbol{\omega}} \times \boldsymbol{r}_{\text{rel}} - m\boldsymbol{\omega} \times (\boldsymbol{\omega} \times \boldsymbol{r}_{\text{rel}}) - 2m(\boldsymbol{\omega} \times \boldsymbol{v}_{\text{rel}}), \qquad (31)$$

where $\boldsymbol{v}_{\text{rel}}$ and $\boldsymbol{r}_{\text{rel}}$ are the velocity and position of the element with respect to the local reference frame, respectively.

For a rotating rotor we have $\boldsymbol{a} = 0$, $\boldsymbol{\omega} = \Omega\boldsymbol{i}$ (with $\boldsymbol{i}$ the unit vector in axial direction) and $\dot{\boldsymbol{\omega}} \approx 0$ (except when starting up). The fictitious forces are recognized as the centrifugal force $m\Omega^2 r$ and the Coriolis force $2m\Omega v$. The centrifugal force is directed outwards, moving fluid elements into the direction of the tip. The Coriolis force on this spanwise velocity component is directed towards the trailing edge and 'helps' to push the fluid against the pressure gradient, delaying stall.

Earth-fixed. For more advanced simulations that include the tower of the turbine or that consider multiple turbines (like for wind farms), it is necessary to have a reference frame fixed to the Earth. This reference frame is often considered to be inertial, because the rotational speed of the Earth

around its axis is small ($\Omega \approx 7.3 \cdot 10^{-5}$ rad/s). When large velocities or large scales are considered, fictitious forces might become important.

Consider a local reference frame rotating with Ω with respect to an inertial reference frame centered in the Earth. Obviously $\boldsymbol{a} = 0$, furthermore Ω is constant so that $\dot{\boldsymbol{\omega}} = 0$ and lastly $\boldsymbol{\omega} \times (\boldsymbol{\omega} \times \boldsymbol{r}_{rel}) = \mathcal{O}(\Omega^2 r_{\mathrm{rel}})$ and can be neglected if r_{rel} is not very large. Therefore only one extra term, the Coriolis term $2(\boldsymbol{\omega} \times \boldsymbol{u})$, is added to the Navier-Stokes equations:

$$\frac{D\boldsymbol{u}}{Dt} = -\frac{1}{\rho}\nabla p + \nu\nabla^2\boldsymbol{u} - 2(\boldsymbol{\omega} \times \boldsymbol{u}). \tag{32}$$

It is expected that for the relatively low velocities considered in wind turbine aerodynamics this term is small with respect to the convective term $\frac{D\boldsymbol{u}}{Dt}$. However, for farm-farm interaction or for modeling the effect of the geostrophic wind this term is not negligible.

4.2.2 Modeling of the rotor

Generalized actuator disk approach. The concept of power extraction by an actuator disk (section 2.2) or actuator line is used by many Navier-Stokes codes as input for near or far wake calculations. It circumvents the modeling of the rotor blades explicitly, reducing the computational cost and easing the mesh generation. The force that the actuator disk exerts on the flow is explicitly added to the momentum equation,

$$\frac{D\boldsymbol{u}}{Dt} = \boldsymbol{f} - \frac{1}{\rho}\nabla p + \nu\nabla^2\boldsymbol{u}. \tag{33}$$

This force $\boldsymbol{f}$ follows from an engineering type method (chapter 3) like BEM, i.e. from tabular data of the lift and drag coefficient for the airfoil profile under consideration. It depends on the local angle of attack, i.e. the local velocity field, and can be time-dependent. The clear bottleneck is the quality with which $\boldsymbol{f}$ can be represented. A general expression for $\boldsymbol{f}$ in two dimensions can be written as:

$$\boldsymbol{f} = (L, D)^T = \frac{1}{2}\rho V^2 c(c_l, c_d)^T, \tag{34}$$

for convenience taken in the direction of lift and drag. A number of problems are inherent in this formulation. First it is difficult to determine V (lift and drag coefficients in wind tunnels are calculated based on the freestream u_∞), and secondly c_l and c_d are functions of α, which is (especially for three-dimensional flow) hard to determine. Other disadvantages were already mentioned in section 3.1.2.
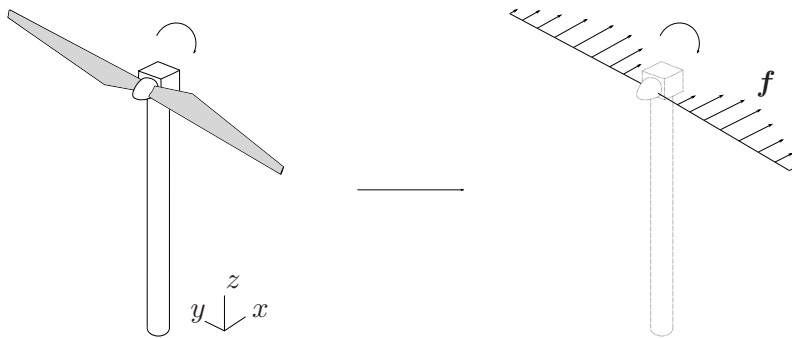
Figure 12: Illustration of the actuator line concept.

Masson and co-workers have used this actuator disk concept [3, 47]. In their approach the actuator disk is seen as a permeable surface (a singularity) on which a (time-averaged) distribution of

forces acts. In [47] the tower is also modeled as a 'permeable' surface. The forces on this surface follow from the experimental value of the drag coefficient of a cylinder. Actually, they prescribe the pressure jump over the discontinuity instead of a force, because it ensures better convergence. The model is three-dimensional and a so-called control-volume finite element method is used.

J.N. Sørensen and others used the actuator disk approach for axisymmetric computations; first in combination with a vorticity-streamfunction formulation for the Euler equations [69] and later also a vorticity-velocity formulation for the Navier-Stokes equations [71].

The *actuator line* approach is somewhat more sophisticated than the actuator disk, since the forces act on rotating lines that represent the blades, instead of being averaged over the entire disk, see figure 12. A regularization kernel is needed to transfer the line forces to the mesh, which is often a trade-off between stability and accuracy. The group of J.N. Sørensen introduced this approach [52, 70] and has recently used it in combination with LES [76, 77], and with 'DNS' (at a lower Reynolds number) [30]. They switched to primitive variables and are implementing all the work in EllipSys3D, a general purpose three-dimensional solver for elliptic partial differential equations.

Recently, the group of J.N. Sørensen extended the actuator line method to an *actuator surface* method [61, 62]. Whereas in the actuator line model an airfoil section is represented by a single point, in the actuator surface model it is represented by a plate on which distributed forces act. In this way the flow cannot cross the chord of the airfoil, which it can in the point approximation of the actuator line technique. This approach has also been taken by Dobrev et al. [20], who couple Fluent with a BEM module that calculates a simplified chordwise pressure distribution.

Direct modeling. The direct modeling of the rotor by constructing a body-fitted grid is physically the most sound method to calculate the flow around a turbine. The challenge that is faced is to minimize its computational cost. Isolated rotors and rotor-hub-tower combinations have been simulated in this way by Duque et al. [21] by using the thin-layer Navier-Stokes approximation and an overset (also known as chimera) grid method (OVERFLOW).

N.N. Sørensen ($k - \omega$ SST) [74] and Johansen (DES) [33] have performed simulations for the NREL rotor (see section 4.3.2) with a rotor-fixed reference frame.

An overset grid method was used by Zahle and N.N. Sørensen to investigate the influence of the tip vortices in the wake on the velocity at the rotor plane [89] and the influence of the tower in downwind [88] and upwind [90] configuration, using fully turbulent flow. One of the interesting pictures they obtained is shown in figure 14, where we see the dependence of accurately calculating tip vortices on grid resolution, the break up of the root vortices after 3 D and the tip vortex break up after 4-6 D.

Comparison of actuator methods and direct modeling has been performed by Réthoré et al. [58]. They show that (at least for uniform inflow) the difference between the two approaches is relatively small and does not justify the significant extra computational effort needed for the full rotor computations.

Transition and turbulence modeling. When directly modeling the rotor, laminar/turbulent transition and turbulence modeling are very important. The most widely used turbulence model is the $k - \omega$ SST model developed by Menter. The CFD group of NRG (no publication yet) used this model for simulations of Delft and MEXICO wind tunnel tests. Conclusions from that work were that transition was predicted too late, and 'simple' calculations by Xfoil showed better transition prediction.
N.N. Sørensen uses the $\gamma - \widetilde{Re_\theta}$ transition model (Langtry-Menter [51]) and finds that transitional computations give better results than fully turbulent simulations [72]. His 2D computations involve already half a million cells on the finest grid, such that a y^+ value of 0.25 is reached. This
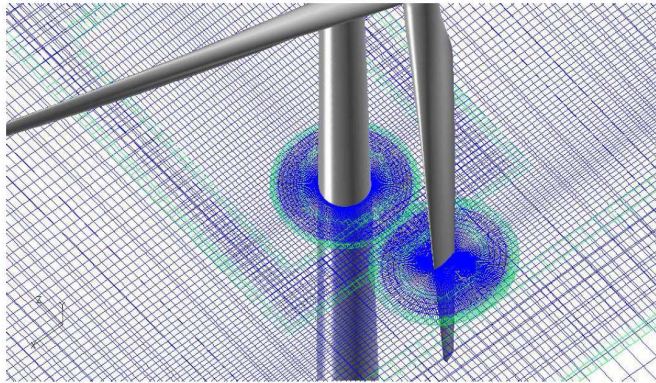
Figure 13: Overset grid used in simulation of Zahle [89].

shows again that in three dimensions such computations become very expensive. In CFX simulations by people from Siemens [38] a similar comparison between this Langtry-Menter model and a fully turbulent flow model was made. It was shown that the application of the transition model lead to a more realistic performance of the blade: increased lift, lowered drag.

4.2.3 Modeling of the wake

The first field models (see section 3.4) made assumptions like axial symmetry or constant advective velocity to simplify the calculations. Ainslie [2] uses a parabolic eddy viscosity model (EVMOD), with zero tangential velocity (axial symmetry), steady flow, and negligible pressure gradients in the outer flow. A Gaussian velocity profile is used as starting condition and the solution is advanced by moving forward in wind direction. Because of this parabolic approach these models have also been called *boundary layer wake models*. Improvements have been made by using a variable-length near wake [35]. Reasonable results are obtained when compared to wind tunnel experiments, but due to the assumption of axial symmetry the downward movement of wake centerline and upwind movement of maximum turbulence intensity cannot be predicted.
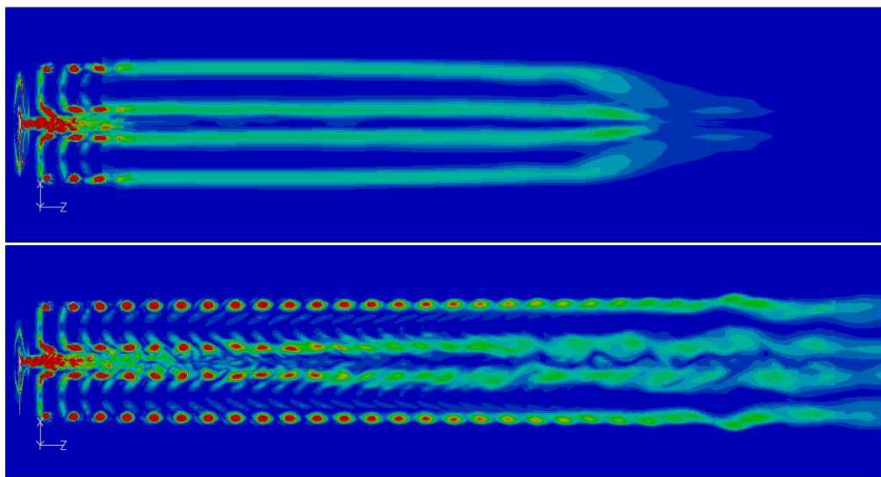
Figure 14: Propagation of tip vortices in the wake for two different wake resolutions. Upper: fine grid until 1 D downstream; lower: entire domain fine grid. No tower, no atmospheric boundary layer, fully turbulent inflow [89].

A more advanced parabolic code is from Crespo and Hernández [13], UPMWAKE, which does not assume axial symmetry and uses a $k - \epsilon$ turbulence model. The parabolicity leads to a fast

solution procedure, but the downside is that the model is not applicable in the near wake, because the axial pressure gradient (an elliptic effect) is neglected. Diffusive effects in axial direction are also neglected. Comparison with the commercial PHOENICS code gave similar results. The UPMWAKE code was used at ECN to develop the WAKEFARM code, which was subsequently improved by including the axial pressure gradient via a boundary layer analogy and coupling it to the near wake via a vortex wake method.

Crespo and Hernández [14] also extended the parabolic code to a fully elliptic version to resolve discrepancies with experimental results that are mainly found in the near-wake region. However, as was also found with other elliptic models, '*any improvement in the agreement with experiments when comparing elliptic and parabolic codes is only slight and does not seem to justify the additional computational effort needed*' [16]. This is an important conclusion, although one should remember it is based on simulations done more than 10 years ago.

A version of UPMWAKE that takes into account the non-isotropic nature of the turbulence in the atmosphere and the wake, UPMANIWAKE, was made recently by Gómez-Elvira, Crespo, and others [23]. They use an explicit algebraic model for the components of the turbulent stress tensor. However, they assume the near wake to be fully turbulent and their analysis is carried out for a neutral atmosphere. They suggest that future improvements can be made by using LES. In fact, Jimenez and Crespo [31] developed a simple LES model with the rotor represented by a simple porous disk on which a force f acts (section 4.2.2) which only depends on the thrust coefficient of the entire rotor. In later work they also took into account shear inflow and looked at the spectral coherence in the wake [32].

The UPMWAKE code was extended to UPMPARK to calculate parks with many turbines [12].

Several authors (e.g. [40]) have retained the Coriolis force in the model, equation (32), and then balance pressure gradients with the Coriolis forces (geostrophic wind, section 2.1.1), but this is not correct since the length scale of the wake is not sufficiently large for Coriolis forces to be significant.

A hybrid method by Magnussen et al. [42] employs a vortex-particle approach in the rotor region, an axisymmetric solver of the turbulent Navier-Stokes equations in the near wake and self preservation (kinematic model) in the far wake.

In the ENDOW [60] and UPWIND [4] projects several wake models have been compared with experimental data. Recently the UPWIND flow package compared models from ECN (WAKE-FARM), GH WindFarmer, CRES/NTUA, CENER (Fluent) and Risø (WaSP). The sub-tasks of this work package which are interesting for the current review are: large offshore wind farms (models and CFD, comparison); wakes in complex terrain (wake interaction with ABL, wake turning, wind-rose narrowing); data assembly / distribution (data for wake model comparison, offshore & complex terrain); reducing wake effects (close spacing, heat & flux, controlling wind, wind farm control).

The work of Larsen et al. focuses at wake meandering by combining both engineering and CFD models [36, 37]. The wake deficits ('cascade elements') are assumed to be passive tracers, that convect downstream with the mean wind speed and move laterally and vertically according to large scale lateral and vertical turbulence velocities in the rotor plane. The wake deficit itself is modeled either with a boundary layer model or a vortex method (see section 4.2.3), which were found to agree well with generalized actuator disk simulations while having much lower computational costs. The wake turbulence is modeled both analytically (extended Joukowski vortex model) and numerically (LES with actuator line), which were used to construct low-dimensional turbulence models via proper orthogonal decomposition (POD) and spectral approaches [68], [36]. In this way the turbulent velocity field is decomposed in a number of modes, and it is shown that a relatively small number of POD modes is necessary to reconstruct the turbulent velocity field. Another feature of their work is that they use periodic boundary conditions to model the effect of many turbines in a row.
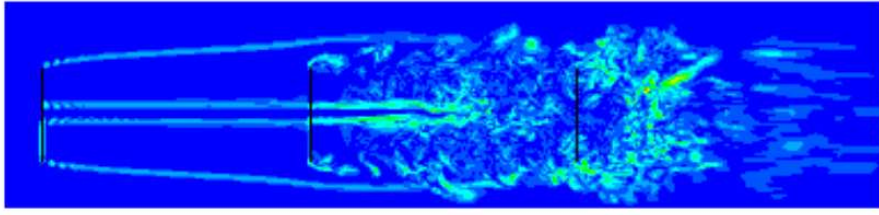
Figure 15: Development of the wake behind three rotors in a row [36]. $u_\infty = 10m/s$, $\lambda = 7$; turbine spacing 3 D.

Farm simulations. In the recent thesis of Ivanell [29] the EllipSys3D code is used to carry out wake and farm simulations, based on the actuator disc/line approach. The atmospheric boundary layer is imposed with the force field technique of Mikkelsen and atmospheric turbulence is generated with Mann's method (see section 4.2.6). The most impressive result from this work is probably the simulation of the Horns Rev wind farm, see figure 16. Twenty actuator discs, in combination with periodic boundary conditions, are used to simulate the 80 turbines of Horns Rev. The power production of downstream turbines agrees reasonably well with experimental data, see figure 17. Discrepancies mainly occur for small inflow angles (the turbines are standing in line at an inflow angle of 270 degrees) and are attributed to the fact that the measured data are based on sectors of ± 2.5 degrees. Improvements can be expected by using the actuator line technique, which is able to generate tip vortices (although this is more expensive). Note that the number of cells for such a simulation is $\mathcal{O}(10^7)$, and that individual cells have a size which is of $\mathcal{O}(1)$m.

CRES and CENER have also performed CFD calculations on an entire wind farm in complex terrain for the UPWIND project, which are not published yet. Some results on complex terrain are available from EWEC 2008 [57].
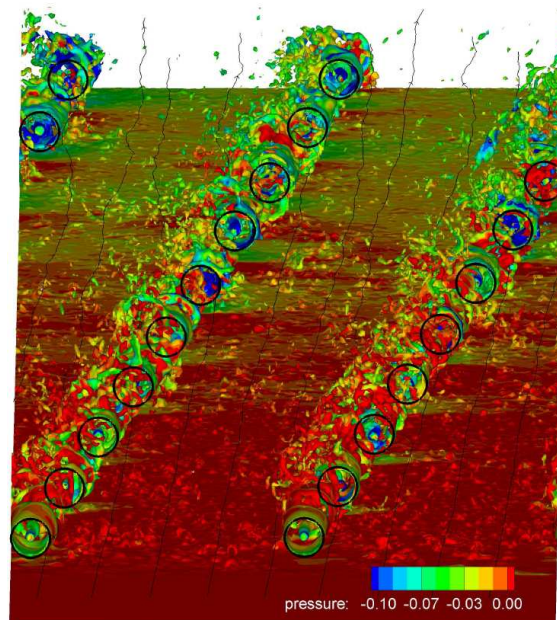
Figure 16: CFD simulation with EllipSys3D of Horns Rev [29].

Vortex methods. A different class of methods that can be used for wake simulations are *vortex methods*. Instead of the regular Eulerian approach commonly encountered in CFD calculations, they are based on a Lagrangian description of the flow field, in which particles model vortex
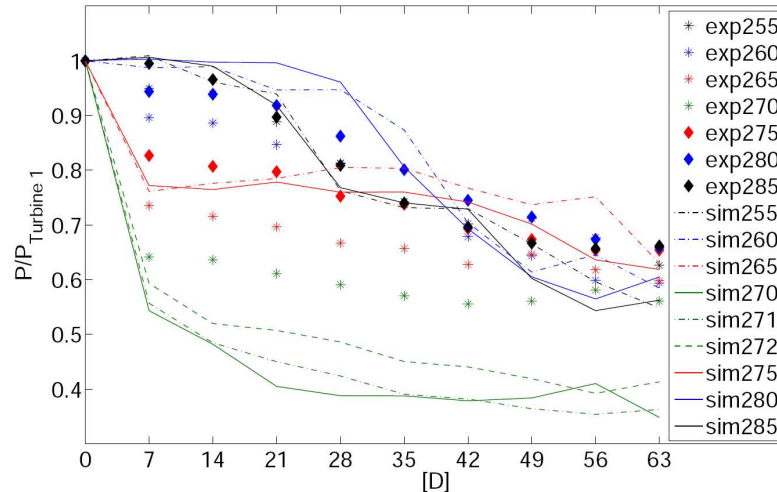
Figure 17: Simulation results compared with measurements for different inflow angles [29].

cores. Vortex methods have been used a few times in the application to wind turbines.

The advantages of the Lagrangian formulation are that there are no difficulties associated with the treatment of the non-linear convection term, as present in the Eulerian formulation. In this way any numerical dissipation, inherently involved in stabilizing the non-linear term in Eulerian formulations, is avoided. The Lagrangian formulation furthermore does not suffer from time step limitations usually found in grid-based discretizations. Other advantages are that the far field is explicitly taken into account, that no pressure term is present and that they are grid-free. Vortex methods require the solution of an N-particle problem, requiring $\mathcal{O}(N^2)$ computations, which becomes excessive for 3D applications (current algorithms require $\mathcal{O}(N \log N)$ computations). Furthermore, vortices have to be spread over the entire computational domain in order to represent the atmospheric boundary layer, and application of boundary conditions is not straightforward, especially for viscous flow.

Zervos et al. [91] used a vortex method to simulate the flow around a single wind turbine and around two turbines in a row. The geometry of the blades was taken into account with a lifting-line method. Only inviscid simulations are performed, but it can easily take into account unsteady and non-uniform flows. Continuation of this work in Greece resulted in the generalized unsteady vortex particle method (GENUVP) by Voutsinas et al., see e.g. [84]. For the near wake a 'normal' vortex wake method is used, based on vortex sheets that leave the blades. In the far wake the vortex sheets change into vortex particles that are calculated with a vortex particle method. Magnusson et al. [42] use such a method for the rotor region instead of the far wake.

A vortex method has been used in the dynamic wake meandering model of Larsen et al. [36], where it is used to calculate the velocity deficit in the wake [54]. Although viscosity is not taken into account, it is very well possible to handle yawed conditions, effects of shear, the merger of turbine wakes and wake instabilities. A pulsating actuator disc model is used, from which tip- and root-vortex rings are emitted. These vortices then move according to the Biot-Savart law. Small disturbances are added to trigger the Kelvin-Helmholtz instability. The results show relatively good agreement in the near wake with calculations based on an actuator-line technique with LES.

Walther et al. [85] use a vortex method to investigate the stability of helical vortices using vortex methods. They perform both inviscid and viscous simulations and show that viscosity destabilizes the vortical system. The calculations are done with 67 million particles and 512 processors.

4.2.4 Modeling of the tower and nacelle

With the use of overset grids, a reduction in thrust and torque of 1-2 % due to the tower shadow was reported by Zahle and N.N. Sørensen [90], as well as signs of dynamic stall behavior on the blades when exiting the shadow. They also investigated the effect of the tower on the blades in case of a downwind configuration [88].
An important parameter is the rotor-tower clearance. How this influences the wake is not fully understood.
Howard and Pereira studied the rotor-tower interaction with LES and a BEM method for the blades [28], and found that the tower influences the flow field upstream of the turbine and generates a wake that is responsible for the destruction of the blade tip vortices.

4.2.5 Techniques used in helicopter wake simulations

The simulation of helicopter rotors faces similar challenges as the simulation of wind turbines, being accurately tracking vortices. For helicopters, the vortex system stays close to the rotor and alters the effective angle of attack. For this purpose, overset grids have been used already since the early 90s, whereas such simulations for wind turbines have only recently been performed (see 4.2.2).

Hariharan and Sankar [26] outline the advantages of using high order Essentially Non Oscillatory (ENO) schemes to capture wake vorticity. In helicopter simulations this is especially interesting due to the occurrence of transonic flow, but in incompressible flow ENO is also useful for high order approximation of the convective terms. By combining a seventh order ENO scheme with a self-adapting vortex-capturing grid, vortices could be accurately tracked for at least 50 chord lengths. Not using the vortex-capturing grid would reduce this length by almost a factor 3, and using a fifth order scheme instead of seventh order by another factor of 3.

Another technique that has been applied for helicopter rotors is called 'Vorticity Confinement' method, a method that modifies the momentum equations to prevent vortex diffusion [75]. It is able to track vortices accurately over long distances, can handle turbulent flow, and allows easy implementation of immersed boundaries. Even on coarse grids it can capture most of the main features of high Reynolds number flows.

Lastly, Discontinuous Galerkin (DG) methods, such as applied by Boelens et al. [8] on the inviscid flow over a helicopter rotor, can be interesting for wind turbine simulations. Its main features are adaptive h/p- refinement (high order) and parallelization.

A difference with wind turbine wakes is that turbulence is not so important in helicopter wakes. Moreover, the atmospheric boundary layer is not important. Lagrangian techniques for the far wake, such as vortex methods, are therefore better applicable because the largest part of the flow field is irrotational.

4.2.6 Boundary conditions

Vermeer [81] mentions that '*One of the most important difficulties that has not been treated satisfactorily is the choice of appropriate input parameters to define ambient unperturbed flow*'. In early CFD simulations uniform inflow profiles were used. However, the presence of the shear inflow profile (boundary layer) has a pronounced effect on the flowfield behind the rotor [90], as well as the turbulence in the incoming flow [77]. The integrated rotor thrust and power for sheared inflow on the other hand were almost identical to those of uniform inflow simulations, although this might depend on the shape of the shear.

Turbulence inflow conditions have been modeled using turbulence models of Mann [44, 45] or the older Sandia-model of Veers [80]. These methods are based on the construction of spectral

tensors as mentioned in section 2.1.3. Mann's algorithm is capable of simulating all three velocity components of a 3D incompressible turbulence field, being homogeneous, stationary, Gaussian, anisotropic and having the same second order statistics as the atmosphere. Troldborg uses this model to create a sheared inflow profile and turbulence in the flow. The velocity field is not directly imposed, but introduced via body forces in the momentum equation in order to maintain a divergence-free velocity field [76, 77].

Recently, a more advanced atmospheric turbulence model was created by Bechmann [6]. In his work an LES model is incorporated in the EllipSys3D code, with switching to a RANS solver to handle the high Reynolds number flow near the surface. Such an LES model can better resemble the anisotropy of the atmospheric turbulence [73].

At ECN the program SWIFT is available, documented in 1996 [87]. It is not based on the principles of fluid mechanics (too expensive, certainly at that time) but instead the simulation scheme is based on a simplified, empirical, statistical model of atmospheric turbulence. The selected algorithm for generating a realization of the stochastic wind field with the required statistical characteristics is the so-called 'Spectral Representation Method'. The basic idea is to specify discrete values of the spectra and cross-spectra and then to calculate the Inverse Discrete Fourier Transform (IDFT) and so generate discrete time sequences which are regarded as sampled values of the continuous random signals required.

If the presence of the Earth is modeled, it should be represented by a no-slip boundary in principle. However, slip (symmetry) conditions have also been used, e.g. [90], by superposing a boundary layer profile on the flow.

At the upper boundary often symmetry conditions are prescribed, at the lateral boundary conditions symmetry or periodicity, and at the outflow a pressure condition or sometimes a periodicity condition is used. A better boundary conditions in these cases might be the so-called 'chimney' condition, which allows for both inflow and outflow.

4.3   Verification and validation

In order to verify CFD results it is necessary to have numerical data to compare with. Comparison with accurate numerical data is needed to find programming errors, evaluate the computational effort, evaluate the order of accuracy of a discretization method and the necessary mesh size. In this way *discretization* and *iterative errors* can be evaluated.
Then, the process of validation can start, i.e. a comparison with experimental data should be made to investigate the quality of the model and to find *model errors*.

4.3.1   Verification - numerical data

A number of well known benchmark test cases exist for verification of incompressible viscous flow, for example:

- Diffusion of multiple vortex system (exact solution, evaluate numerical diffusion).

- Flow over a backward-facing step (separation, recirculation bubble, reattachment).

- Flow over a cylinder (separation, vortex street, unsteady).

- Flow over an oscillating cylinder (moving bodies).

- Flow over an airfoil (high Reynolds number flow).

4.3.2 Validation - experimental data

Experimental data can be categorized into two classes: field tests (open air) and wind tunnel tests.

Wind tunnel tests.   Wind tunnel tests on rotating wind turbine models are the most suitable source of experimental data as verification for numerical simulation because they take place in a controlled environment. However, scaling and blocking effects should be taken into account when interpreting the data, and it is hard to reproduce the atmospheric conditions encountered in reality, including the Reynolds number. Turbulence intensity in a wind tunnel is often lower, and the length of the near wake is then overestimated. Ainslie mentions that the velocity deficits are larger in wind tunnel experiments, but he relates it to wake meandering that occurs in the field.

An elaborate overview of near- and far-wake experiments is given in Vermeer [81]. Two of these are mentioned here:

- The 'best' experiment to date is the NREL Unsteady Aerodynamic Experiment in the NASA Ames 80ft x 120ft wind tunnel [63], with a 10m rotor diameter ('full-scale'), performed in 2000. The results were ('blindly') compared with numerical simulations. Serious shortcomings in the BEM models were revealed, but the Navier-Stokes simulations showed better agreement. However, no wake measurements were done during these tests.

- ECN has performed wind tunnel tests in the DNW (December 2006), on a 4.5m diameter rotor in a 9.5mx9.5m test section, in the context of the MEXICO project. Near-wake measurements are available (from -1 D to 1.5 D, with PIV), as well as pressure recordings on the blades. A joint effort in which the Mexico measurements are evaluated is performed in the (currently ongoing) MEXNEXT project.

Field tests.   Field tests have been cataloged in a database by IEA, Annex XVIII. Again, a problem of field measurements is that the inflow is continuously changing and often not (fully) known, and the number of measurement stations is limited. However, it is the only way to obtain data on full-scale wind turbines influencing each other in a farm.
Well-known experimental data are the Tjæreborg turbine [55], the Nibe turbine, the Sexbierum measurements [11]. For groups of turbines well known test cases are Horns Rev, Nysted, Middlegrunden, Vindeby, EWTW (ECN test site). Not all data is publicly available.

5 Optimization

As mentioned in the introduction, this report will not focus on optimization. We will only shortly mention what the problem is about and where the difficulties lie.

Literature on the optimization of wind farms that includes aerodynamic effects is scarce. One of the few examples is the work of Beyer [7] which uses genetic algorithms for optimization and an engineering method for the aerodynamics of the wake. Other studies have been performed on the optimization of wind farms that have installation and maintenance cost as objective function. A more interesting objective function would be the total power P of a wind farm divided by the cost. P is a function of the individual wind turbine locations x_i and their operational settings σ_i (thrust coefficient, yaw angle, turbine height, diameter, ...):

$$P = f(x_i, \sigma_i). \tag{35}$$

The mathematical formulation of the optimization problem can be stated as:

$$\max_{x_i, \sigma_i} f(x_i, \sigma_i) \quad \text{subject to} \quad g(x_i, \sigma_i) \leq 0, \tag{36}$$

where g represents the constraints, e.g. the operating characteristics of the wind turbines. Boundary conditions for the problem are given by the shape and surface area of the terrain. The function f is expected to depend non-linearly on its arguments due to the non-linear nature of the Navier-Stokes equations. This non-linearity, together with the possible existence of local maxima, makes the problem challenging.

6 Summary

In this report the existing literature on the calculation of wind turbine wakes is reviewed. First, as introduction to wind turbine aerodynamics, in chapter 2 the aerodynamic flow features of a wind turbine are discussed. The (stability of the) atmospheric boundary layer and the ambient turbulence are important in calculating the velocity field and turbulence intensity behind wind turbines, as well as the terrain layout and surface roughness. The important distinction between near and far wake is explained, including the different physical processes that occur in these regions. The recovery of the velocity deficit and turbulent fluctuations in the far wake depends on thrust coefficient and ambient turbulence level. The latter is noticeable further downstream. In wind farms the loss in power of the second turbine row is in general significant when standing in line with the wind direction, but for successive turbines the power loss is much smaller. The turbulence in the successive wakes becomes saturated, and an equilibrium value is reached.

It is believed that due to the variability in wind direction and the presence of large-scale atmospheric eddies the wake starts to meander, which is important in calculating the mutual influence of turbines in farms.

In chapter 3 different engineering models for fast prediction of both rotor performance and wake aerodynamics were discussed. The blade element momentum method is the most widely used method for rotor computations, while for wake calculations many codes use superposition of velocity deficits and turbulent kinetic energies. However, computational fluid dynamics (chapter 4) is continuously attracting more attention because it can provide a more accurate and detailed prediction of the flow field.

The mathematical model for wind farm aerodynamics simulations should be the unsteady, viscous, incompressible Navier-Stokes equations. In order to relieve computer requirements these equations have often been solved in a parabolized sense. However, in order to calculate the near wake and to correctly simulate the mutual influence of wind turbines in a park the full equations should be solved. Solving the full equations has been the trend for the last years, and the main complexity now lies in correctly modeling the turbulent nature of the flow. The 'best' turbulence model that can correctly take into account the anisotropy in the flow is LES, although the computational requirements for wind farms are still quite high. This is the reason that RANS simulations are widely in use, but a common problem is that they overpredict the amount of diffusion in the wake (at least for the $k - \epsilon$ model). Due to the high Reynolds numbers it is hard to simulate correctly the real viscous phenomena without creating numerical dissipation.

Calculations of the entire rotor, tower and wake have been performed with overset grids, but they are too expensive for wind farm aerodynamics and simpler models should be used to represent the rotor. A widely used technique is the actuator approach, in which the rotor is represented by forces. These forces depend on the flow field and are obtained from tabulated airfoil data. The first steady actuator disk computations have now evolved to unsteady actuator line and actuator surface techniques. The actuator technique has been successfully used for the simulation of entire wind farms.

For such calculations a model for the turbulent atmosphere is needed as a boundary condition. Currently the model of Mann is the standard way of generating turbulence.

Optimization of wind farm layouts with current CFD codes is not yet possible due to the large computational effort already required for a single wind farm computation.

References

[1] J.F. Ainslie. Development of an eddy-viscosity model for wind turbine wakes. In *Proceedings of the 7th BWEA conference*, pages 61–65, 1985.

[2] J.F. Ainslie. Calculating the field in the wake of wind turbines. *Journal of Wind Engineering and Industrial Aerodynamics*, 27:213–224, 1988.

[3] I. Ammara, C. Leclerc, and C. Masson. A viscous three-dimensional method for the aerodynamic analysis of wind farms. *Journal of Solar Energy Engineering*, 124:345–356, 2002.

[4] R.J. Barthelmie, S.T. Frandsen, K. Hansen, J.G. Schepers, K. Rados, W. Schlez, A. Neubert, L.E. Jensen, and S. Neckelmann. Modelling the impact of wakes on power output at Nysted and Horns Rev. In *European Wind Energy Conference*, 2009.

[5] R.J. Barthelmie, S.T. Frandsen, O. Rathmann, K. Hansen, E.S. Politis, J. Prospathopoulos, D. Cabezón, K. Rados, S.P. van der Pijl, J.G. Schepers, W. Schlez, J. Phillips, and A. Neubert. Flow and wakes in large wind farms in complex terrain and offshore. In *European Wind Energy Conference*, 2008.

[6] A. Bechmann. *Large-eddy simulation of atmospheric flow over complex terrain*. PhD thesis, Technical University of Denmark, 2006.

[7] H. G. Beyer, T. Rüger, G. Schäfer, and H.-P. Waldl. Optimization of wind farm configuration with variable number of turbines. In *Proceedings European Union Wind Energy Conference, Göteborg*, pages 1073–1076, 1996.

[8] O. J. Boelens, H. van der Ven, B. Oskam, and A. A. Hassan. Boundary conforming discontinuous Galerkin finite element approach for rotorcraft simulations. *Journal of Aircraft*, 39(5):776–785, 2002.

[9] E.A. Bossanyi, C. Maclean, G.E. Whittle, P.D. Dunn, N.H. Lipman, and P.J. Musgrove. The efficiency of wind turbine clusters. In *Proceedings of the 3rd Symposium on Wind Energy Systems*, pages 401–416, 1980.

[10] T. Burton, D. Sharpe, N. Jenkins, and E. Bossanyi. *Wind energy handbook*. John Wiley & Sons, 2001.

[11] J.W. Cleijne. Results of Sexbierum wind farm; single wake measurements. Technical Report TNO-Report 93-082, TNO Institute of Environmental and Energy Technology, 1993.

[12] A. Crespo, L. Chacón, J. Hernández, F. Manuel, and J.C. Grau. UPMPARK: a parabolic 3D code to model wind farms. In *Proceedings of EWEC 1994*, pages 454–459.

[13] A. Crespo and J. Hernández. Numerical modelling of the flow field in a wind turbine wake. In *Proceedings of the 3rd Joint ASCE/ASME Mechanics Conference*, pages 121–127. ASME, 1989.

[14] A. Crespo and J. Hernández. Parabolic and elliptic models of wind turbine wakes. application to the interaction between different wakes and turbines. *PHOENICS Journal of Computational Fluid Dynamics*, 4:104–127, 1991.

[15] A. Crespo and J. Hernández. Turbulence characteristics in wind-turbine wakes. *Journal of Wind Engineering and Industrial Aerodynamics*, 61:71–85, 1996.

[16] A. Crespo, J. Hernández, and S. Frandsen. Survey of modelling methods for wind turbine wakes and wind farms. *Wind Energy*, 2:1–24, 1999.

[17] A. Crespo, F. Manuel, D. Moreno, E. Fraga, and J. Hernandez. Experimental validation of the UPM computer code to calculate wind turbine wakes and comparison with other models. In *Proceedings of Delphi Workshop on Wind Energy Applications, Delphi, Greece*, pages 15–25, 1985.

[18] J.A. Dahlberg, M. Poppen, and S.E. Thor. Load/fatigue life effects on a wind turbine generator in a wind farm. In *European Wind Energy Conference*, 1991.

[19] P.A. Davidson. *Turbulence - an introduction for scientists and engineers*. Oxford University Press, 2004.

[20] I. Dobrev, F. Massouh, and M. Rapin. Actuator surface hybrid model. *Journal of Physics*, 75, 2007.

[21] E.P.N. Duque, C.P. van Dam, and S.C. Hughes. Navier-Stokes simulations of the NREL combined experiment rotor phase II. AIAA Paper 99-0037, 1999.

[22] D.L. Elliott. Status of wake and array loss research. In *Windpower Conference Palm Springs, California*, 1991.

[23] R. Gómez-Elvira, A. Crespo, E. Migoya, F. Manuel, and J. Hernández. Anisotropy of turbulence in wind turbine wakes. *Journal of Wind Engineering and Industrial Aerodynamics*, 93:797–814, 2005.

[24] M.O.L. Hansen. *Aerodynamics of windturbines*. Earthscan Publications Ltd., 2001.

[25] M.O.L. Hansen, J.N. Sørensen, and W.Z. Shen. Vorticity-velocity formulation of the 3D navier-stokes equations in cylindrical coordinates. *International Journal for Numerical Methods in Fluids*, 41:29–45, 2003.

[26] N. Hariharan and L.M. Sankar. A review of computational techniques for rotor wake modeling. AIAA Paper 00-0114, 2000.

[27] J. Højstrup. Spectral coherence in wind turbine wakes. *Journal of Wind Engineering and Industrial Aerodynamics*, 80:137–146, 1999.

[28] R.J.A. Howard and J.C.F Pereira. A study of wind turbine power generation and turbine-tower interaction using large eddy simulation. *Wind and Structures*, 9(2):95–108, 2006.

[29] S. Ivanell. *Numerical computation of wind turbine wakes*. PhD thesis, KTH Mechanics, Royal Institute of Technology, 2009.

[30] S. Ivanell, J.N. Sørensen, R. Mikkelsen, and D. Henningson. Analysis of numerically generated wake structures. *Wind Energy*, 12:63–80, 2009.

[31] A. Jimenez, A. Crespo, E. Migoya, and J. Garcia. Advances in large-eddy simulation of a wind turbine wake. In *The science of making torque from wind. Conference series*, volume 75, 2007.

[32] A. Jimenez, A. Crespo, E. Migoya, and J. Garcia. Large-eddy simulation of spectral coherence in a wind turbine wake. *Environmental Research Letters*, 3, 2008.

[33] J. Johansen, N.N. Sørensen, J.A. Michelsen, and S. Schreck. Detached-eddy simulation of flow around the NREL phase VI blade. *Wind Energy*, 5:185–197, 2002.

[34] A. El Kasmi and C. Masson. An extended $k-\epsilon$ model for turbulent flow through horizontal-axis wind turbines. *Journal of Wind Engineering and Industrial Aerodynamics*, 96:103–122, 2008.

[35] B. Lange, H. Waldl, A.G. Guerrero, D. Heinemann, and R. J. Barthelmie. Modelling of offshore wind turbine wakes with the wind farm program FLaP. *Wind Energy*, 6:87–104, 2003.

[36] G.C. Larsen, H.A. Madsen, F. Bingöl, J. Mann, S. Ott, J.N. Sørensen, V. Okulov, N. Troldborg, M. Nielsen, K. Thomsen, T.J. Larsen, and R. Mikkelsen. Dynamic wake meandering modeling. Technical Report R-1607, Risø National Laboratory, Technical University of Denmark, 2007.

[37] G.C. Larsen, H.A. Madsen, K. Thomsen, and T.J. Larsen. Wake meandering: a pragmatic approach. *Wind Energy*, 11:377–395, 2008.

[38] J. Laursen, P. Enevoldsen, and S. Hjort. 3D CFD quantification of the performance of a multi-megawatt wind turbine. In *The science of making torque from wind. Conference series*, volume 75, 2007.

[39] P.B.S. Lissaman. Energy effectiveness of arbitrary arrays of wind turbines. AIAA Paper 79-0114, 1979.

[40] M.-K. Liu, M.A. Yocke, and T.L. Myers. Mathematical model for the analysis of wind-turbine wakes. *Journal of Energy*, 7:73–78, 1983.

[41] H.A. Madsen, G.C. Larsen, and K. Thomsen. Wake flow characteristics in low ambient turbulence conditions. In *Copenhagen Offshore Wind*, 2005.

[42] M. Magnusson, K.G. Rados, and S.G. Voutsinas. A study of the flow downstream of a wind turbine using measurements and simulations. *Wind Engineering*, 20(6):389–403, 1996.

[43] M. Magnusson and A.-S. Smedman. Air flow behind wind turbines. *Journal of Wind Engineering and Industrial Aerodynamics*, 80:169–189, 1999.

[44] J. Mann. The spatial structure of neutral atmospheric surface-layer turbulence. *Journal of Fluid Mechanics*, 273:141–168, 1994.

[45] J. Mann. Wind field simulation. *Probabilistic engineering mechanics*, 13(4):269–282, 1998.

[46] J.F. Manwell, J.G. McGowan, and A.L. Rogers. *Wind energy explained*. John Wiley & Sons, 2002.

[47] C. Masson, A. Smaïli, and C. Leclerc. Aerodynamic analysis of HAWTs operating in unsteady conditions. *Wind Energy*, 4:1–22, 2001.

[48] B.W. McCormick. *Aerodynamics of V/STOL flight*. Dover Publications Inc., 1999.

[49] D. Medici. *Experimental studies of wind turbine wakes - power optimisation and meandering*. PhD thesis, KTH Mechanics, Royal Institute of Technology, 2005.

[50] D. Medici and P.H. Alfredsson. Measurements behind model wind turbines: further evidence of wake meandering. *Wind Energy*, 11:211–217, 2008.

[51] F.R. Menter, R.B. Langtry, S.R. Likki, Y.B. Suzen, P.G. Huang, and S. Völker. A correlation-based transition model using local variables, part i - model formulation. *ASME Journal of Turbomachinery*, 128(3):413–422, 2006.

[52] R. Mikkelsen. *Actuator disc methods applied to wind turbines*. PhD thesis, Technical University of Denmark, 2002.

[53] H.E. Neustadter and D.A. Spera. Method for evaluating wind turbine wake effects on wind farm performance. *Journal of Solar Energy Engineering*, 107:240–243, 1985.

[54] S. Ott. A vorticity based approach to wind turbine wake modelling. Technical Report R-1618, Risø National Laboratory, Technical University of Denmark, 2007.

[55] S. Oye. Tjaereborg wind turbine, first dynamic inflow measurements. Technical Report AFM Notak Vk-189, Technical University of Denmark, 1991.

[56] H.A. Panofsky and J.A. Dutton. *Atmospheric Turbulence*. Wiley, 1984.

[57] J. M. Prospathopoulos, E. S. Politis, and P. K. Chaviaropoulos. Modelling wind turbine wakes in complex terrain. In *Proceedings EWEC 2008, Brussels, Belgium*, 2008.

[58] P.-E. Réthoré, N.N. Sørensen, F. Zahle, and J. Johansen. Comparison of an actuator disc model with a full rotor cfd model under uniform and shear inflow condition. In *Book of abstracts; 4th PhD seminar on wind energy in Europe, Magdeburg*, pages 123–126, 2008.

[59] J.G. Schepers. ENDOW: Validation and improvement of ECN's wake model. Technical Report ECN-C-03-034, Energy research Centre of the Netherlands, 2003.

[60] W. Schlez, A. Umana, R. Barthelmie, G. Larsen, K. Rados, B. Lange, G. Schepers, and T. Hegberg. ENDOW: Improvement of wake models within offshore wind farms. *Wind Engineering*, 25:281–287, 2001.

[61] W.Z. Shen, J.N. Sørensen, and J.H. Zhang. Actuator surface model for wind turbine flow computations. In *Proceedings EWEC 2007*, 2007.

[62] W.Z. Shen, J.H. Zhang, and J.N. Sørensen. The actuator-surface model: a new Navier-Stokes based model for rotor computations. *Journal of Solar Energy Engineering*, 131, 2009.

[63] D. Simms, S. Schreck, M. Hand, and L.J. Fingersh. NREL unsteady aerodynamics experiment in the NASA-Ames wind tunnel: a comparison of predictions to measurements. Technical Report NREL/TP-500-29494, NREL - National Renewable Energy Laboratory, June 2001.

[64] D. Smith and G.J. Taylor. Further analysis of turbine wake development and interaction data. In *Proceedings of the 13th BWEA Wind Energy Conference, Swansea, UK*, pages 325–331, 1991.

[65] H. Snel. Review of the present status of rotor aerodynamics. *Wind Energy*, 1:46–69, 1998.

[66] H. Snel. Review of aerodynamics for wind turbines. *Wind Energy*, 6:203–211, 2003.

[67] J.N. Sørensen and C.W. Kock. A model for unsteady rotor aerodynamics. *Journal of Wind Engineering and Industrial Aerodynamics*, 58:259–275, 1995.

[68] J.N. Sørensen, R. Mikkelsen, and N. Troldborg. Simulation and modeling of turbulence in wind farms. In *Proceedings EWEC 2007*, 2007.

[69] J.N. Sørensen and A. Myken. Unsteady actuator disc model for horizontal axis wind turbines. *Journal of Wind Engineering and Industrial Aerodynamics*, 39:139–149, 1992.

[70] J.N. Sørensen and W.Z. Shen. Numerical modeling of wind turbine wakes. *Journal of Fluids Engineering*, 124:393–399, 2002.

[71] J.N. Sørensen, W.Z. Shen, and X. Munduate. Analysis of wake states by a full-field actuator disc model. *Wind Energy*, 1:73–88, 1998.

[72] N.N. Sørensen. CFD modeling of laminar-turbulent transition for airfoils and rotors using the $\gamma - \widetilde{Re_\theta}$ model. In *26th AIAA Applied Aerodynamics Conference, Honolulu, Hawaii*, 2008.

[73] N.N. Sørensen and J. Johansen. UPWIND, aerodynamics and aero-elasticity. Rotor aerodynamics in atmospheric shear flow. In *Proceedings EWEC 2007*, 2007.

[74] N.N. Sørensen, J.A. Michelsen, and S. Schreck. Navier-Stokes predictions of the NREL phase VI rotor in the NASA Ames 80ft x 120ft wind tunnel. *Wind Energy*, 5:151–169, 2002.

[75] J. Steinhoff, W. Yonghu, and W. Lesong. Computation of separating high Reynolds number incompressible flows using vorticity confinement. In *14th Computational Fluid Dynamics Conference, Norfolk*, 1999.

[76] N. Troldborg. *Actuator line modeling of wind turbine wakes*. PhD thesis, Technical University of Denmark, 2008.

[77] N. Troldborg, J.N. Sørensen, and R. Mikkelsen. Actuator line simulation of wake of wind turbine operating in turbulent inflow. In *The science of making torque from wind. Conference series*, volume 75, 2007.

[78] S.P. van der Pijl. Numerical modeling of wind farm aerodynamics, June 2007. ECN internal report.

[79] A. van Garrel. Development of a wind turbine aerodynamics simulation module. Technical Report ECN-C-03-079 EN, Energy research Centre of the Netherlands, 2003.

[80] P.S. Veers. Three-dimensional wind simulation. Technical Report SAND88-0152, Sandia National Laboratories, 1988.

[81] L.J. Vermeer, J.N. Sørensen, and A. Crespo. Wind turbine wake aerodynamics. *Progress in Aerospace Sciences*, 39:467–510, 2003.

[82] N.J. Vermeer. How big is a tip vortex? In *Proceedings 10th IEA symposium on aerodynamics of wind turbines*, 1996.

[83] P.E.J. Vermeulen. An experimental analysis of wind turbine wakes. In *Proceedings of the 3rd Symposium on Wind Energy Systems*, pages 431–450, 1980.

[84] S.G. Voutsinas, M.A. Belessis, and S. Huberson. Dynamic inflow effects and vortex particle methods. In *European Wind Energy Conference Proceedings*, pages 428–431, 1993.

[85] J.H. Walther, M. Guénot, E. Machefaux, J.T. Rasmussen, P. Chatelain, V.L. Okulov, J.N. Sørensen, M. Bergdorf, and P. Koumoutsakos. A numerical study of the stability of helical vortices using vortex methods. In *The science of making torque from wind. Conference series*, volume 75, 2007.

[86] J. Whale, C.G. Anderson, R. Bareiss, and S. Wagner. An experimental and numerical study of the vortex structure in the wake of a wind turbine. *Journal of Wind Engineering and Industrial Aerodynamics*, 84:1–21, 2000.

[87] D. Winkelaar. Ontwikkeling van een stochastisch windbelastingmodel, deel 1: Windmodellering (in Dutch). Technical Report ECN-C-96-096, 1996.

[88] F. Zahle, J. Johansen, N.N. Sørensen, and J.M.R. Graham. Wind turbine rotor-tower interaction using an incompressible overset grid method. AIAA Paper 2007-425, 2007.

[89] F. Zahle and N.N. Sørensen. On the influence of far-wake resolution on wind turbine flow simulations. In *The science of making torque from wind. Conference series*, volume 75, 2007.

[90] F. Zahle and N.N. Sørensen. Overset grid flow simulation on a modern wind turbine. AIAA Paper 2008-6727, 2008.

[91] A. Zervos, S. Huberson, and A. Hemon. Three-dimensional free wake calculation of wind turbine wakes. *Journal of Wind Engineering and Industrial Aerodynamics*, 27:65–76, 1988.